Chinese Journal of Aeronautics, (2017), 30(3): 1071–1085

Chinese Society of Aeronautics and Astronautics
& Beihang University

Chinese Journal of Aeronautics

cja@buaa.edu.cn
www.sciencedirect.com

Robust attitude coordinated control for spacecraft formation with communication delays

Jian ZHANG [a], **Qinglei HU** [b,*], **Danwei WANG** [c], **Wenbo XIE** [d]

[a] *Department of Control Science and Engineering, Harbin Institute of Technology, Harbin 150001, China*
[b] *School of Automation Science and Electrical Engineering, Beihang University, Beijing 100083, China*
[c] *School of Electrical and Electronic Engineering, Nanyang Technological University, Singapore 639798, Singapore*
[d] *College of Automation, Harbin University of Science and Technology, Harbin 150080, China*

Received 24 May 2016; revised 26 September 2016; accepted 31 October 2016
Available online 15 February 2017

KEYWORDS

Actuator saturation;
Attitude control;
Communication delays;
Neural networks;
Spacecraft formation

Abstract In this paper, attitude coordinated tracking control algorithms for multiple spacecraft formation are investigated with consideration of parametric uncertainties, external disturbances, communication delays and actuator saturation. Initially, a sliding mode delay-dependent attitude coordinated controller is proposed under bounded external disturbances. However, neither inertia uncertainty nor actuator constraint has been taken into account. Then, a robust saturated delay-dependent attitude coordinated control law is further derived, where uncertainties and external disturbances are handled by Chebyshev neural networks (CNN). In addition, command filter technique is introduced to facilitate the backstepping design procedure, through which actuator saturation problem is solved. Thus the spacecraft in the formation are able to track the reference attitude trajectory even in the presence of time-varying communication delays. Rigorous analysis is presented by using Lyapunov-Krasovskii approach to demonstrate the stability of the closed-loop system under both control algorithms. Finally, the numerical examples are carried out to illustrate the efficiency of the theoretical results.

1. Introduction

Spacecraft formation flying has become an attractive topic during the last decade, and extensive effort has been put on this novel technique theoretically and practically. From the existing research literatures, a large number of advantages of the decentralized control algorithms have been shown, such as better system reliability and higher robustness. The control architectures for formation coordination can be categorized into four types, namely, the leader-follower structure,[1] the behavioral based approach,[2] the virtual structure[3] and graph-theoretical based technique.[4]

Practically speaking, the spacecraft formation subjects to various uncertainties such as the unknown disturbance and the time-varying inertia moment. Yang et al.[5] accomplished accuracy estimation of the external disturbances by using an

* Corresponding author.
E-mail address: huql_buaa@buaa.edu.cn (Q. HU).
Peer review under responsibility of Editorial Committee of CJA.

http://dx.doi.org/10.1016/j.cja.2017.01.014
1000-9361

extended observer. Considering parametric uncertainties and disturbances, Zhang et al.[6] proposed a sliding mode and adaptive coordinated tracking controller for multiple rigid spacecraft. As for a group of flexible spacecraft, Du and Li[7] employed backstepping control approach to solve the attitude synchronization problem. Neural networks (NNs) show effective performance to approximate the continuous functions over any arbitrary accuracy, which makes it be a favorable technique in nonlinear system controller design. Based on Chebyshev neutral network, Zou et al.[8] proposed a robust control law for the spacecraft in the presence of unknown inertia moment and external disturbances. Fazlyab et al.[9] designed an adaptive fault-tolerant controller for a rigid spacecraft by three-layered neutral network approximation technique. Zhao and Jia[10] developed a finite-time attitude synchronization control algorithm for multiple spacecraft formation by utilizing neural networks and modified fast terminal sliding mode.

Apart from the issues stated above, input saturation caused by the limitation of actuator is another challenge for spacecraft attitude maneuver.[11–20] Su and Zheng[13] proposed globally asymptotic saturated control laws for spacecraft attitude stabilization by modifying traditional proportional-derivative controller. Boskovic et al.[14] constructed a time-varying sliding mode control scheme to achieve attitude stabilization for spacecraft under input saturation and uncertainties. Bustan et al.[15] applied the similar approach to design fault-tolerant attitude tracking control law for a rigid spacecraft. Loria and Nijeijer[16] adopted hyperbolic tangent function to derive bounded output feedback for Euler-Lagrange system. Homogenous system theory combined with hyperbolic tangent function was used to obtain the finite-time coordinated control algorithms for a group of spacecraft formation in Refs. [18, 19]. Zou and Kumar[20] investigated attitude coordinated control problem for multiple spacecraft, where neural network was employed and an auxiliary signal was used to compensate the exceeding value of control torque.

Moreover, time-delay is unavoidable whenever information transfers between neighboring spacecraft due to communication bandwidth limitation and obstructions in space. The ignorance of such phenomenon may degrade control performance and bring unpredictable effect to system stability. Under such circumstance, the need for developing control algorithms with consideration of the communication delays arises. Li and Liu[21] derived the adaptive sliding mode control laws for spacecraft formation with uncertainties and constant non-uniform delays. Zhou et al.[22] proposed a velocity-free decentralized attitude synchronization algorithm with time-varying delays. On basis of the previous research works, coordinated control schemes for spacecraft formation under directed communication topology were carried out. Regardless of external disturbance and parametric uncertainties, Li et al.[23] designed control law by using backstepping technique and finite-time method. The uncertain factors were also neglected in Ref. [24]. For the purpose of handling system uncertainties and unknown disturbances, adaptive attitude synchronization control laws were investigated in the presence of communication delays.[25–27] Especially, Du and Li[27] proposed attitude synchronized control law for multiple flexible spacecraft, where finite-time control technique was also involved. More recently, input saturation has been considered in the time-delay systems as well. Xu et al.[28] proposed a robust controller for uncertain discrete time-delay system with bounded external disturbances and input saturation. Abdessameud and Tayebi[29] studied synchronization algorithm for Euler-Lagrange systems with communication delays, where the upper bound of control input was related to control gains and the number of formation members. It is worth emphasizing that extending these results to spacecraft formation attitude coordinated problem is not straightforward owing to the inherent coupled nonlinear dynamics of spacecraft.

Inspired by the previous research works, we concentrate on developing attitude coordinated tracking control laws for spacecraft formation with communication delay, external disturbance, inertia uncertainties and even actuator constraints. Although attitude coordinated control problem for spacecraft formation has been widely studied, control strategy taking these above factors into consideration simultaneously can hardly be found, especially when the communication topology is directed. First, a sliding mode attitude coordinated controller is presented for a formation subjected to environmental disturbance, where communication delays are considered explicitly. Then, CNN approximation approach is applied to enhance system robustness to uncertainties and disturbances. Backstepping technique with command filter has been adopted to develop the robust saturated control law. Additionally, the information exchange topology between neighboring spacecraft is supposed to be directed, which not only leads to practical significance but also poses more challenges on controller design.

The organization of this paper is as follows. In Section 2, mathematical model of spacecraft formation attitude system and some preliminaries on graph theory are presented. The main work is stated in Section 3, where two novel attitude coordinated control laws are derived and sufficient conditions for system stability are obtained. Then, the effectiveness of the theoretical results is verified by numerical examples in the following section. Finally, the conclusion and remarks are made in Section 5.

2. Preliminaries

2.1. Spacecraft formation attitude kinematics and dynamics

Unit quaternion is introduced for attitude kinematics of the ith spacecraft[30]

$$\dot{q}_{i0} = -\frac{1}{2}\boldsymbol{q}_i^{\mathrm{T}}\boldsymbol{\omega}_i \tag{1}$$

$$\dot{\boldsymbol{q}}_i = \boldsymbol{Q}(\boldsymbol{q}_i)\boldsymbol{\omega}_i = \frac{1}{2}(q_{i0}\boldsymbol{I}_{3\times 3} + \boldsymbol{q}_i^{\times})\boldsymbol{\omega}_i \tag{2}$$

The dynamic model of the ith spacecraft is governed by

$$\boldsymbol{J}_i\dot{\boldsymbol{\omega}}_i + \boldsymbol{\omega}_i^{\times}\boldsymbol{J}_i\boldsymbol{\omega}_i = \boldsymbol{u}_i + \boldsymbol{d}_i \tag{3}$$

where $\bar{\boldsymbol{q}}_i = [q_{i0}, \boldsymbol{q}_i^{\mathrm{T}}]^{\mathrm{T}} \in \mathbf{R}^4$ is the quaternion denoting the rotation from the body frame of the spacecraft to the inertial frame, q_{i0} and $\boldsymbol{q}_i \in \mathbf{R}^3$ satisfy $\boldsymbol{q}_i^{\mathrm{T}}\boldsymbol{q}_i + q_{i0}^2 = 1$; $\boldsymbol{\omega}_i \in \mathbf{R}^3$ is the angular velocity expressed in the body frame; $\boldsymbol{J}_i \in \mathbf{R}^{3\times 3}$ represents the inertia tensor; $\boldsymbol{u}_i \in \mathbf{R}^3$ and $\boldsymbol{d}_i \in \mathbf{R}^3$ denote the control torque and environmental disturbances acting on the ith spacecraft, respectively.

As attitude coordinated tracking problem is addressed in this article, the reference trajectory for the spacecraft forma-

tion is described by $\bar{\boldsymbol{q}}_{\mathrm{d}} = [q_{\mathrm{d}0}, \boldsymbol{q}_{\mathrm{d}}^{\mathrm{T}}]^{\mathrm{T}} \in \mathbf{R}^4$ with the desired angular velocity $\boldsymbol{\omega}_{\mathrm{d}} \in \mathbf{R}^3$. The attitude tracking error $\bar{\boldsymbol{q}}_{\mathrm{e}i} = [q_{\mathrm{e}i0}, \boldsymbol{q}_{\mathrm{e}i}^{\mathrm{T}}]^{\mathrm{T}} \in \mathbf{R}^4$ and angular velocity tracking error $\boldsymbol{\omega}_{\mathrm{e}i} \in \mathbf{R}^3$ are introduced, which are defined as $\bar{\boldsymbol{q}}_{\mathrm{e}i} = \bar{\boldsymbol{q}}_{\mathrm{d}}^{-1} \odot \bar{\boldsymbol{q}}_i$ and $\boldsymbol{\omega}_{\mathrm{e}i} = \boldsymbol{\omega}_i - \boldsymbol{R}_{\mathrm{e}i}\boldsymbol{\omega}_{\mathrm{d}}$. $\boldsymbol{R}_{\mathrm{e}i} = (q_{\mathrm{e}i0}^2 - \boldsymbol{q}_{\mathrm{e}i}^{\mathrm{T}}\boldsymbol{q}_{\mathrm{e}i})\boldsymbol{I}_{3\times3} + 2\boldsymbol{q}_{\mathrm{e}i}\boldsymbol{q}_{\mathrm{e}i}^{\mathrm{T}} - 2q_{\mathrm{e}i0}\boldsymbol{q}_{\mathrm{e}i}^{\times}$ represents the rotation matrix from the body frame to the reference frame. Let $\boldsymbol{Q}(\boldsymbol{q}_{\mathrm{e}i}) = \frac{1}{2}(q_{\mathrm{e}i0}\boldsymbol{I}_{3\times3} + \boldsymbol{q}_{\mathrm{e}i}^{\times})$, which is denoted as $\boldsymbol{Q}_{\mathrm{e}i}$ for brevity and satisfies $\|\boldsymbol{Q}_{\mathrm{e}i}\| = \frac{1}{2}$, and we obtain

$$\dot{q}_{\mathrm{e}i0} = -\frac{1}{2}\boldsymbol{q}_{\mathrm{e}i}^{\mathrm{T}}\boldsymbol{\omega}_{\mathrm{e}i} \tag{4}$$

$$\dot{\boldsymbol{q}}_{\mathrm{e}i} = \boldsymbol{Q}(\boldsymbol{q}_{\mathrm{e}i})\boldsymbol{\omega}_{\mathrm{e}i} \tag{5}$$

$$\begin{aligned}\boldsymbol{J}_i\dot{\boldsymbol{\omega}}_{\mathrm{e}i} = {} & -(\boldsymbol{\omega}_{\mathrm{e}i} + \boldsymbol{R}_{\mathrm{e}i}\boldsymbol{\omega}_{\mathrm{d}})^{\times}\boldsymbol{J}_i(\boldsymbol{\omega}_{\mathrm{e}i} + \boldsymbol{R}_{\mathrm{e}i}\boldsymbol{\omega}_{\mathrm{d}}) - \boldsymbol{J}_i(\boldsymbol{R}_{\mathrm{e}i}\dot{\boldsymbol{\omega}}_{\mathrm{d}} \\ & - \boldsymbol{\omega}_{\mathrm{e}i}^{\times}\boldsymbol{R}_{\mathrm{e}i}\boldsymbol{\omega}_{\mathrm{d}}) + \boldsymbol{u}_i + \boldsymbol{d}_i\end{aligned} \tag{6}$$

Assumption 1. The external disturbance $\boldsymbol{d}_i$ is assumed to be bounded, i.e. $\|\boldsymbol{d}_i\| \leqslant d_{\mathrm{M}}$ with d_{M} being a positive constant.

Assumption 2. The desired angular velocity $\boldsymbol{\omega}_{\mathrm{d}}$ and its first-time derivative $\dot{\boldsymbol{\omega}}_{\mathrm{d}}$ are supposed to be bounded.

2.2. Graph theory

We assume that the information exchange of the spacecraft formation is described by a fixed and directed graph $G(\boldsymbol{A}) \cong \{V, E, \boldsymbol{A}\}$. Each spacecraft is denoted as a node in the graph, and $V = \{v_i\}$ $(i = 1, 2, \ldots, n)$ denotes the set of nodes. $E \subseteq V \times V$ presents the set of the edges and $\boldsymbol{A} = [a_{ij}] \in \mathbf{R}^{n\times n}$ is the adjacency matrix of the graph with non-negative adjacency elements a_{ij}. The directed edge $(v_i, v_j) \in E$ exits if there is an available information channel from the ith spacecraft to the jth spacecraft, and thus it has $a_{ij} > 0$ correspondingly. Otherwise $a_{ij} = 0$, if node i and node j are not connected. Besides, it is supposed that $a_{ii} = 0$ for all $i = 1, 2, \ldots, n$. The Laplacian matrix of the graph G is defined as $\boldsymbol{L}^* = [l_{ij}^*] \in \mathbf{R}^{n\times n}$, where $l_{ii}^* = \sum_{j=1}^n a_{ij}$ and $l_{ij}^* = -a_{ij}$ where $i \neq j$.

Assumption 3. Throughout this paper, the communication graph G of the formation is supposed to be fixed and directed, and contains a spanning tree. Moreover, the reference information can be reached by at least one spacecraft in the formation.

Lemma 1. [31] *If the directed graph G has a spanning tree, then* 0 *is a simple eigenvalue of $\boldsymbol{L}^*$ with $\boldsymbol{I}_N$ as its right eigenvector, and all the other $N-1$ eigenvalues have positive real parts.*

3. Main results

As the main results of this paper, two novel distributed attitude tracking control algorithms are proposed for the spacecraft formation with communication delays. First, a sliding mode control law is proposed on the condition that the inertia matrices can be measured accurately and there is no constraint on the actuator torque. Then, improvements are made to accomplish the control objective of developing a bounded control law with high robustness. Neural network is involved to handle the system parametric uncertainties and the external disturbances. Backstepping technique with command filter is adopted to solve input saturation.

3.1. Delay-dependent attitude coordinated controller design

In this subsection, the inertia matrix $\boldsymbol{J}_i$ is supposed to be precisely known as a prior. The sliding mode manifold $\boldsymbol{s}_{\mathrm{e}i} = \boldsymbol{\omega}_{\mathrm{e}i} + \varepsilon\boldsymbol{q}_{\mathrm{e}i}$ is employed with ε being a positive constant. For the ith spacecraft, a sliding mode delay-dependent attitude coordinated control algorithm is proposed:

$$\begin{aligned}\boldsymbol{u}_i = {} & -\boldsymbol{\omega}_{\mathrm{e}i}^{\times}\boldsymbol{J}_i\boldsymbol{\omega}_{\mathrm{e}i} + \boldsymbol{\omega}_i^{\times}\boldsymbol{J}_i\boldsymbol{\omega}_i + \boldsymbol{J}_i(\boldsymbol{R}_{\mathrm{e}i}\dot{\boldsymbol{\omega}}_{\mathrm{d}} - \boldsymbol{\omega}_{\mathrm{e}i}^{\times}\boldsymbol{R}_{\mathrm{e}i}\boldsymbol{\omega}_{\mathrm{d}}) \\ & - \rho\mathrm{sgn}(\boldsymbol{s}_{\mathrm{e}i}) - k_1\boldsymbol{\omega}_{\mathrm{e}i} - k_2\boldsymbol{q}_{\mathrm{e}i} - k_3|\lambda_{\max}(\boldsymbol{L}\boldsymbol{L}^{\mathrm{T}})|\boldsymbol{s}_{\mathrm{e}i} \\ & - k_3\sum_{j=1}^{n} a_{ij}(\boldsymbol{q}_{\mathrm{e}i}(t-T) - \boldsymbol{q}_{\mathrm{e}j}(t-T))\end{aligned} \tag{7}$$

where T denotes time-varying communication delays between the neighboring spacecraft, which always satisfies $1 - \dot{T} > 0$; $\boldsymbol{L} = \boldsymbol{L}^* \otimes \boldsymbol{I}_{3\times3}$ and $\lambda_{\max}(\boldsymbol{L}\boldsymbol{L}^{\mathrm{T}})$ denotes the maximum eigenvalue of matrix $\boldsymbol{L}\boldsymbol{L}^{\mathrm{T}}$; the robust control term $-\rho\mathrm{sgn}(\boldsymbol{s}_{\mathrm{e}i})$ is introduced to restrain external disturbance with the positive constant ρ satisfying $\rho > d_{\mathrm{M}}$; the control gains k_1, k_2 and k_3 are positive constants satisfying $2(k_2 + \varepsilon k_1)\lambda_{\min}(\boldsymbol{J}) \geqslant \varepsilon^2\lambda_{\max}^2(\boldsymbol{J})$, where $\lambda_{\min}(\boldsymbol{J})$ and $\lambda_{\max}(\boldsymbol{J})$ denote the minimum and maximum eigenvalue of matrix $\boldsymbol{J}$ and $\boldsymbol{J} = \mathrm{diag}(\boldsymbol{J}_1, \boldsymbol{J}_2, \ldots, \boldsymbol{J}_n)$.

In order to address the stability of systems with time-delays, the following lemmas are given.

Lemma 2. [32] *For a continuous function $\varpi(x)$ and its derivative $\dot{\varpi}(x)$ defined on $[a, b]$, we have*

$$\int_a^b \dot{\varpi}(x)\mathrm{d}x = \varpi(b) - \varpi(a)$$

Lemma 3. [32] *For any symmetric positive definite matrix $\boldsymbol{M} \in \mathbf{R}^{n\times n}$, constants r_1 and r_2 satisfy $r_1 < r_2$, and the vector function $\boldsymbol{\upsilon} : [r_1, r_2] \to \mathbf{R}^n$ such that*

$$\int_{r_1}^{r_2} \boldsymbol{\upsilon}^{\mathrm{T}}(s)\boldsymbol{M}\boldsymbol{\upsilon}(s)\mathrm{d}s \geqslant \frac{1}{r_{12}}\left(\int_{r_1}^{r_2}\boldsymbol{\upsilon}(s)\mathrm{d}s\right)^{\mathrm{T}}\boldsymbol{M}\left(\int_{r_1}^{r_2}\boldsymbol{\upsilon}(s)\mathrm{d}s\right)$$

where $r_{21} = r_2 - r_1$.

Theorem 1. *Considering spacecraft formation governed by Eqs. (1)–(3), if the sliding mode attitude coordinated controller Eq. (7) is adopted and the system parameters are selected to satisfy the following inequalities,*

$$2k_2\varepsilon - k_3 > 0 \tag{8}$$

$$k_1 - \frac{1}{2}\varepsilon\lambda_{\max}(\boldsymbol{J}) - 1 - T + \dot{T} > 0 \tag{9}$$

$$\frac{1}{T} - \frac{1}{8}k_3 > 0 \tag{10}$$

Then, the closed-loop system achieves asymptotically stable, i.e. the attitude error and angular velocity error of each spacecraft converge to zero asymptotically.

Proof. Substituting controller Eq. (7) into Eq. (6) and rewriting the closed-loop system into vector form lead to

$$\begin{aligned}\boldsymbol{J}\dot{\boldsymbol{\omega}}_{\mathrm{e}} = &-\boldsymbol{\omega}_{\mathrm{e}}^{\times}\boldsymbol{J}\boldsymbol{\omega}_{\mathrm{e}} - \rho\mathrm{sgn}(\boldsymbol{s}_{\mathrm{e}}) - k_1\boldsymbol{\omega}_{\mathrm{e}} - k_2\boldsymbol{q}_{\mathrm{e}} \\ &- k_3|\lambda_{\max}(\boldsymbol{L}\boldsymbol{L}^{\mathrm{T}})|\boldsymbol{s}_{\mathrm{e}} - k_3\boldsymbol{L}\left(\boldsymbol{q}_{\mathrm{e}} - \int_{t-T}^{t}\dot{\boldsymbol{q}}_{\mathrm{e}}\mathrm{d}\sigma\right) + \boldsymbol{d} \end{aligned} \tag{11}$$

where Lemma 2 is used and the vectors $\boldsymbol{s}_{\mathrm{e}} = [\boldsymbol{s}_{\mathrm{e}1}^{\mathrm{T}}, \boldsymbol{s}_{\mathrm{e}2}^{\mathrm{T}}, \ldots, \boldsymbol{s}_{\mathrm{e}n}^{\mathrm{T}}]^{\mathrm{T}}$, $\boldsymbol{q}_{\mathrm{e}} = [\boldsymbol{q}_{\mathrm{e}1}^{\mathrm{T}}, \boldsymbol{q}_{\mathrm{e}2}^{\mathrm{T}}, \ldots, \boldsymbol{q}_{\mathrm{e}n}^{\mathrm{T}}]^{\mathrm{T}}$, $\boldsymbol{\omega}_{\mathrm{e}} = [\boldsymbol{\omega}_{\mathrm{e}1}^{\mathrm{T}}, \boldsymbol{\omega}_{\mathrm{e}2}^{\mathrm{T}}, \ldots, \boldsymbol{\omega}_{\mathrm{e}n}^{\mathrm{T}}]^{\mathrm{T}}$ and $\boldsymbol{d} = [\boldsymbol{d}_1^{\mathrm{T}}, \boldsymbol{d}_2^{\mathrm{T}}, \ldots, \boldsymbol{d}_n^{\mathrm{T}}]^{\mathrm{T}}$ are defined.

A Lyapunov function is constructed as

$$\begin{aligned}V_1 = &\frac{1}{2}\boldsymbol{\omega}_{\mathrm{e}}^{\mathrm{T}}\boldsymbol{J}\boldsymbol{\omega}_{\mathrm{e}} + \varepsilon\boldsymbol{q}_{\mathrm{e}}^{\mathrm{T}}\boldsymbol{J}\boldsymbol{\omega}_{\mathrm{e}} + 2(k_2+\varepsilon k_1)\sum_{i=1}^{n}(1-q_{\mathrm{e}i0}) \\ &+ \int_{t-T}^{t}\boldsymbol{\omega}_{\mathrm{e}}^{\mathrm{T}}\boldsymbol{\omega}_{\mathrm{e}}\mathrm{d}\sigma + \int_{-T}^{0}\int_{t+\zeta}^{t}\boldsymbol{\omega}_{\mathrm{e}}^{\mathrm{T}}\boldsymbol{\omega}_{\mathrm{e}}\mathrm{d}\sigma\mathrm{d}\zeta \end{aligned} \tag{12}$$

Due to the fact that $1 + q_{\mathrm{e}i0} \in (0, 2)$, it can be obtained that

$$\begin{aligned}V_1 \geqslant &\frac{1}{2}\lambda_{\min}(\boldsymbol{J})\boldsymbol{\omega}_{\mathrm{e}}^{\mathrm{T}}\boldsymbol{\omega}_{\mathrm{e}} - \varepsilon\lambda_{\max}(\boldsymbol{J})\|\boldsymbol{q}_{\mathrm{e}}^{\mathrm{T}}\boldsymbol{\omega}_{\mathrm{e}}\| + 2(k_2+\varepsilon k_1)\sum_{i=1}^{n}\frac{\boldsymbol{q}_{\mathrm{e}i}^{\mathrm{T}}\boldsymbol{q}_{\mathrm{e}i}}{1+q_{\mathrm{e}i0}} \\ &+ \int_{t-T}^{t}\boldsymbol{\omega}_{\mathrm{e}}^{\mathrm{T}}\boldsymbol{\omega}_{\mathrm{e}}\mathrm{d}\sigma + \int_{-T}^{0}\int_{t+\zeta}^{t}\boldsymbol{\omega}_{\mathrm{e}}^{\mathrm{T}}\boldsymbol{\omega}_{\mathrm{e}}\mathrm{d}\sigma\mathrm{d}\zeta \\ \geqslant &\frac{1}{2}\left(\sqrt{\lambda_{\min}(\boldsymbol{J})}\boldsymbol{\omega}_{\mathrm{e}} - \frac{\varepsilon\lambda_{\max}(\boldsymbol{J})}{\sqrt{\lambda_{\min}(\boldsymbol{J})}}\boldsymbol{q}_{\mathrm{e}}\right)^2 + \left(k_2+\varepsilon k_1 - \frac{\varepsilon^2\lambda_{\max}^2(\boldsymbol{J})}{2\lambda_{\min}(\boldsymbol{J})}\right)\boldsymbol{q}_{\mathrm{e}}^{\mathrm{T}}\boldsymbol{q}_{\mathrm{e}} \\ &+ \int_{t-T}^{t}\boldsymbol{\omega}_{\mathrm{e}}^{\mathrm{T}}\boldsymbol{\omega}_{\mathrm{e}}\mathrm{d}\sigma + \int_{-T}^{0}\int_{t+\zeta}^{t}\boldsymbol{\omega}_{\mathrm{e}}^{\mathrm{T}}\boldsymbol{\omega}_{\mathrm{e}}\mathrm{d}\sigma\mathrm{d}\zeta \end{aligned} \tag{13}$$

Obviously, V_1 is proved to be positive and definite if $2(k_2 + \varepsilon k_1)\lambda_{\min}(\boldsymbol{J}) \geqslant \varepsilon^2\lambda_{\max}^2(\boldsymbol{J})$ holds. Then, taking the time derivative of V_1 gives

$$\begin{aligned}\dot{V}_1 = &(\boldsymbol{\omega}_{\mathrm{e}}^{\mathrm{T}} + \varepsilon\boldsymbol{q}_{\mathrm{e}}^{\mathrm{T}})\left[\boldsymbol{d} - \rho\mathrm{sgn}(\boldsymbol{s}_{\mathrm{e}}) - k_1\boldsymbol{\omega}_{\mathrm{e}} - k_2\boldsymbol{q}_{\mathrm{e}} - k_3|\lambda_{\max}(\boldsymbol{L}\boldsymbol{L}^{\mathrm{T}})|\boldsymbol{s}_{\mathrm{e}}\right. \\ &\left.-k_3\boldsymbol{L}\left(\boldsymbol{q}_{\mathrm{e}} - \int_{t-T}^{t}\dot{\boldsymbol{q}}_{\mathrm{e}}\mathrm{d}\sigma\right)\right] \\ &+\varepsilon\frac{1}{2}\sum_{i=1}^{n}\left[(q_{\mathrm{e}i0}\boldsymbol{I}_{3\times3} + \boldsymbol{q}_{\mathrm{e}i}^{\times})\boldsymbol{\omega}_{\mathrm{e}i}\right]^{\mathrm{T}}\boldsymbol{J}_i\boldsymbol{\omega}_{\mathrm{e}i} - \varepsilon\boldsymbol{q}_{\mathrm{e}}^{\mathrm{T}}\boldsymbol{\omega}_{\mathrm{e}}^{\times}\boldsymbol{J}\omega_{\mathrm{e}} + (k_2+\varepsilon k_1)\boldsymbol{q}_{\mathrm{e}}^{\mathrm{T}}\boldsymbol{\omega}_{\mathrm{e}} \\ &+(1-\dot{T})\boldsymbol{\omega}_{\mathrm{e}}^{\mathrm{T}}\boldsymbol{\omega}_{\mathrm{e}} \quad -(1-\dot{T})\boldsymbol{\omega}_{\mathrm{e}}^{\mathrm{T}}(t-T)\boldsymbol{\omega}_{\mathrm{e}}(t-T) + T\boldsymbol{\omega}_{\mathrm{e}}^{\mathrm{T}}\boldsymbol{\omega}_{\mathrm{e}} \\ &-\int_{t-T}^{t}\boldsymbol{\omega}_{\mathrm{e}}^{\mathrm{T}}\boldsymbol{\omega}_{\mathrm{e}}\mathrm{d}\sigma \\ \leqslant &-k_3|\lambda_{\max}(\boldsymbol{L}\boldsymbol{L}^{\mathrm{T}})|\boldsymbol{s}_{\mathrm{e}}^{\mathrm{T}}\boldsymbol{s}_{\mathrm{e}} - k_1\|\boldsymbol{\omega}_{\mathrm{e}}\|^2 - k_2\varepsilon\|\boldsymbol{q}_{\mathrm{e}}\|^2 \\ &-\boldsymbol{s}_{\mathrm{e}}^{\mathrm{T}}k_3\boldsymbol{L}\left(\boldsymbol{q}_{\mathrm{e}} - \int_{t-T}^{t}\dot{\boldsymbol{q}}_{\mathrm{e}}\mathrm{d}\sigma\right) + \frac{1}{2}\varepsilon\sum_{i=1}^{n}q_{\mathrm{e}i0}\boldsymbol{\omega}_{\mathrm{e}i}^{\mathrm{T}}\boldsymbol{J}_i\boldsymbol{\omega}_{\mathrm{e}i} \\ &+(1+T-\dot{T})\boldsymbol{\omega}_{\mathrm{e}}^{\mathrm{T}}\boldsymbol{\omega}_{\mathrm{e}} - (1-\dot{T})\boldsymbol{\omega}_{\mathrm{e}}^{\mathrm{T}}(t-T)\boldsymbol{\omega}_{\mathrm{e}}(t-T) - \int_{t-T}^{t}\boldsymbol{\omega}_{\mathrm{e}}^{\mathrm{T}}\boldsymbol{\omega}_{\mathrm{e}}\mathrm{d}\sigma \end{aligned} \tag{14}$$

By using Young's inequality,[33] the following inequalities can be verified:

$$\boldsymbol{s}_{\mathrm{e}}^{\mathrm{T}}k_3\boldsymbol{L}\boldsymbol{q}_{\mathrm{e}} \leqslant \frac{1}{2}k_3\boldsymbol{s}_{\mathrm{e}}^{\mathrm{T}}\boldsymbol{L}\boldsymbol{L}^{\mathrm{T}}\boldsymbol{s}_{\mathrm{e}} + \frac{1}{2}k_3\boldsymbol{q}_{\mathrm{e}}^{\mathrm{T}}\boldsymbol{q}_{\mathrm{e}} \tag{15}$$

$$\begin{aligned}\boldsymbol{s}_{\mathrm{e}}^{\mathrm{T}}k_3\boldsymbol{L}\int_{t-T}^{t}\dot{\boldsymbol{q}}_{\mathrm{e}}\mathrm{d}\sigma \leqslant &\frac{1}{2}k_3\boldsymbol{s}_{\mathrm{e}}^{\mathrm{T}}\boldsymbol{L}\boldsymbol{L}^{\mathrm{T}}\boldsymbol{s}_{\mathrm{e}} \\ &+\frac{1}{2}k_3\left(\int_{t-T}^{t}\dot{\boldsymbol{q}}_{\mathrm{e}}\mathrm{d}\sigma\right)^{\mathrm{T}}\left(\int_{t-T}^{t}\dot{\boldsymbol{q}}_{\mathrm{e}}\mathrm{d}\sigma\right) \end{aligned} \tag{16}$$

Given $\dot{\boldsymbol{q}}_{\mathrm{e}} = \boldsymbol{Q}_{\mathrm{e}}\boldsymbol{\omega}_{\mathrm{e}}$, where $\boldsymbol{Q}_{\mathrm{e}} = \mathrm{diag}(\boldsymbol{Q}_{\mathrm{e}1}, \boldsymbol{Q}_{\mathrm{e}2} \ldots, \boldsymbol{Q}_{\mathrm{e}n})$. Noting that $\|\boldsymbol{Q}_{\mathrm{e}}\| = \frac{1}{2}$ and with Lemma 3 in mind, we have

$$\begin{aligned}\left(\int_{t-T}^{t}\dot{\boldsymbol{q}}_{\mathrm{e}}\mathrm{d}\sigma\right)^{\mathrm{T}}\left(\int_{t-T}^{t}\dot{\boldsymbol{q}}_{\mathrm{e}}\mathrm{d}\sigma\right) &= \left(\int_{t-T}^{t}\boldsymbol{Q}_{\mathrm{e}}\boldsymbol{\omega}_{\mathrm{e}}\mathrm{d}\sigma\right)^{\mathrm{T}}\left(\int_{t-T}^{t}\boldsymbol{Q}_{\mathrm{e}}\boldsymbol{\omega}_{\mathrm{e}}\mathrm{d}\sigma\right) \\ &\leqslant \frac{1}{4}\left(\int_{t-T}^{t}\boldsymbol{\omega}_{\mathrm{e}}\mathrm{d}\sigma\right)^{\mathrm{T}}\left(\int_{t-T}^{t}\boldsymbol{\omega}_{\mathrm{e}}\mathrm{d}\sigma\right) \end{aligned} \tag{17}$$

$$\left(\int_{t-T}^{t}\boldsymbol{\omega}_{\mathrm{e}}\mathrm{d}\sigma\right)^{\mathrm{T}}\left(\int_{t-T}^{t}\boldsymbol{\omega}_{\mathrm{e}}\mathrm{d}\sigma\right) \leqslant T\int_{t-T}^{t}\boldsymbol{\omega}_{\mathrm{e}}^{\mathrm{T}}\boldsymbol{\omega}_{\mathrm{e}}\mathrm{d}\sigma \tag{18}$$

Thus we further get

$$\begin{aligned}\dot{V}_1 \leqslant &-k_3\boldsymbol{s}_{\mathrm{e}}^{\mathrm{T}}\left(|\lambda_{\max}(\boldsymbol{L}\boldsymbol{L}^{\mathrm{T}})|\boldsymbol{I}_{3n\times3n} - \boldsymbol{L}\boldsymbol{L}^{\mathrm{T}}\right)\boldsymbol{s}_{\mathrm{e}} - \left(k_2\varepsilon - \frac{1}{2}k_3\right)\|\boldsymbol{q}_{\mathrm{e}}\|^2 \\ &-\left(k_1 - \frac{1}{2}\varepsilon\lambda_{\max}(\boldsymbol{J}) - 1 - T + \dot{T}\right)\|\boldsymbol{\omega}_{\mathrm{e}}\|^2 \\ &-(1-\dot{T})\boldsymbol{\omega}_{\mathrm{e}}^{\mathrm{T}}(t-T)\boldsymbol{\omega}_{\mathrm{e}}(t-T) \\ &-\left(\frac{1}{T} - \frac{1}{8}k_3\right)\left(\int_{t-T}^{t}\boldsymbol{\omega}_{\mathrm{e}}\mathrm{d}\sigma\right)^{\mathrm{T}}\left(\int_{t-T}^{t}\boldsymbol{\omega}_{\mathrm{e}}\mathrm{d}\sigma\right) \end{aligned} \tag{19}$$

If $|\lambda_{\max}(\boldsymbol{L}\boldsymbol{L}^{\mathrm{T}})|\boldsymbol{I}_{3n\times3n} - \boldsymbol{L}\boldsymbol{L}^{\mathrm{T}}$ is positive definite and Eqs. (8)–(10) are satisfied, it can be concluded that $\dot{V}_1 \leqslant 0$. Hence, it causes that V_1 is bounded, which implies $\boldsymbol{\omega}_{\mathrm{e}} \in \mathcal{L}_2 \cap \mathcal{L}_\infty$, $\boldsymbol{q}_{\mathrm{e}} \in \mathcal{L}_2 \cap \mathcal{L}_\infty$, $\boldsymbol{\omega}_{\mathrm{e}}(t-T) \in \mathcal{L}_\infty$ and $q_{\mathrm{e}0} \in \mathcal{L}_\infty$. Recalling the closed-loop system, we get $\dot{\boldsymbol{\omega}}_{\mathrm{e}} \in \mathcal{L}_\infty$. Additionally, it can be proved that $\dot{\boldsymbol{q}}_{\mathrm{e}} \in \mathcal{L}_\infty$ from the kinematic model Eq. (5). By using the Barbalat's lemma,[34] it follows that $\lim_{t\to\infty}\boldsymbol{q}_{\mathrm{e}} = \boldsymbol{0}$ and $\lim_{t\to\infty}\boldsymbol{\omega}_{\mathrm{e}} = \boldsymbol{0}$, i.e. the attitude and angular velocity of each spacecraft converge to the reference trajectory asymptotically. □

Remark 1. Given Lemma 1 and the fact that the communication topology contains a spanning tree, $\lambda_{\max}(\boldsymbol{L}\boldsymbol{L}^{\mathrm{T}})$ is a positive constant. Hence, it leads to $|\lambda_{\max}(\boldsymbol{L}\boldsymbol{L}^{\mathrm{T}})|\boldsymbol{I}_{3n\times3n} - \boldsymbol{L}\boldsymbol{L}^{\mathrm{T}} > \boldsymbol{0}$, which guarantees the above analysis.

Remark 2. In Theorem 1, the inertia tensor $\boldsymbol{J}_i$ is assumed to be known precisely and the limitation of actuator torque has not been considered. However, such assumptions can barely be satisfied in practical cases. Thus, a robust saturated controller is further derived in the following section.

3.2. Robust saturated delay-dependent controller design

In the preceding section, the sliding mode delay-dependent control law is proposed without inertia uncertainties and input saturation. Although the robustness against external disturbance and communication delays is ensured, it is inevitable to bring large gain as the disturbances and uncertainties increase. Nevertheless, the control torque ought to be bounded because of the physical limitation of actuator onboard. There-

fore, the necessity of developing control law with input saturation is obvious.

Before the control algorithms are derived, the following assumption is made.

Assumption 4. The inertia of each spacecraft is divided into $\boldsymbol{J}_i = \boldsymbol{J}_{0i} + \Delta\boldsymbol{J}_i$, where $\boldsymbol{J}_{0i}$ denotes the nominal part and $\Delta\boldsymbol{J}_i$ the uncertain part. The norm of $\boldsymbol{J}_{0i}$ satisfies $\underline{\delta} \leqslant \|\boldsymbol{J}_{0i}^{-1}\| \leqslant \bar{\delta}$ with $\underline{\delta}$ and $\bar{\delta}$ being positive constants.

Then, the kinematic and dynamic model of the spacecraft formation are reformed:

$$\dot{\boldsymbol{v}}_{ei} = \boldsymbol{f}(\boldsymbol{q}_{ei}, \boldsymbol{v}_{ei}) + \boldsymbol{g}_0(\boldsymbol{q}_{ei})\boldsymbol{u}_{0i} + \boldsymbol{d}_i^* = \boldsymbol{D}_i(\cdot) + \boldsymbol{g}_0(\boldsymbol{q}_{ei})\mathrm{sat}(\boldsymbol{u}_i) \tag{20}$$

where $\boldsymbol{v}_{ei} = \dot{\boldsymbol{q}}_{ei}$; $\boldsymbol{f}(\boldsymbol{q}_{ei}, \boldsymbol{v}_{ei}) = \dot{\boldsymbol{Q}}_{ei}\boldsymbol{F}_{ei}\boldsymbol{v}_{ei} - \boldsymbol{Q}_{ei}\boldsymbol{J}_i^{-1}\{(\boldsymbol{F}_{ei}\boldsymbol{v}_{ei} + \boldsymbol{v}_{1i})^{\times}\boldsymbol{J}_i(\boldsymbol{F}_{ei}\boldsymbol{v}_{ei} + \boldsymbol{v}_{1i}) - \boldsymbol{J}_i[(\boldsymbol{F}_{ei}\boldsymbol{v}_{ei})^{\times}\boldsymbol{v}_{1i} - \boldsymbol{v}_{2i}]\} + \tilde{\boldsymbol{g}}(\boldsymbol{q}_{ei})\mathrm{sat}(\boldsymbol{u}_i)$, with $\boldsymbol{F}_{ei} = \boldsymbol{F}(\boldsymbol{q}_{ei}) = \boldsymbol{Q}(\boldsymbol{q}_{ei})^{-1}$, $\boldsymbol{v}_{1i} = \boldsymbol{R}_{ei}\boldsymbol{\omega}_{\mathrm{d}}$, $\boldsymbol{v}_{2i} = \boldsymbol{R}_{ei}\dot{\boldsymbol{\omega}}_{\mathrm{d}}$, $\tilde{\boldsymbol{g}}(\boldsymbol{q}_{ei}) = \boldsymbol{Q}_{ei}(\boldsymbol{J}_i^{-1} - \boldsymbol{J}_{0i}^{-1})$; $\boldsymbol{g}_0(\boldsymbol{q}_{ei}) = \boldsymbol{Q}_{ei}\boldsymbol{J}_{0i}^{-1}$; $\boldsymbol{d}_i^* = g(\boldsymbol{q}_{ei})\boldsymbol{d}_i$, with $\boldsymbol{g}(\boldsymbol{q}_{ei}) = \boldsymbol{Q}_{ei}\boldsymbol{J}_i^{-1}$; $\boldsymbol{D}_i(\cdot) = \boldsymbol{f}(\boldsymbol{q}_{ei}, \boldsymbol{v}_{ei}) + \boldsymbol{d}_i^*$. The saturated torque is denoted as $\boldsymbol{u}_{0i} = \mathrm{sat}(\boldsymbol{u}_i)$, which is further defined as

$$u_{0iw} = \mathrm{sat}(u_{iw}) = \begin{cases} \mathrm{sgn}(u_{iw})\bar{u}_0 & |u_{iw}| > \bar{u}_0 \\ u_{iw} & |u_{iw}| < \bar{u}_0 \end{cases}, \quad w = 1, 2, 3 \tag{21}$$

Thus the signal $\boldsymbol{u}_i$ will be constraint to an allowable scope $\bar{u}_0$ before acting on individual spacecraft.

Remark 3. In the view of $\|\boldsymbol{Q}_{ei}\| = \frac{1}{2}$ and Assumption 4, it is easy to verify that $\boldsymbol{g}_0(\boldsymbol{q}_{ei}) = \boldsymbol{Q}_{ei}\boldsymbol{J}_{0i}^{-1} \leqslant \frac{1}{2}\bar{\delta}$.

Remark 4. Note that $\boldsymbol{F}_{ei}$ will exit when $\boldsymbol{Q}_{ei}$ is invertible, which implies that $\det(\boldsymbol{Q}_{ei}) = \frac{1}{2}q_{ei0}(t) \neq 0$ for $t \geqslant 0$. Thus, the initial state and control strategy should be chosen to guarantee $q_{ei0}(t) \neq 0$ for all time.

From Eq. (20), it can be seen that the nonlinear term $\boldsymbol{D}_i(\cdot)$ is important for system analysis. Given the remarkable performance of neural network for approximating uncertain dynamics and nonlinear functions, the Chebyshev neural network (CNN) is employed to facilitate control law design. Consequently, the unknown function is approximated by

$$\boldsymbol{D}_i(\boldsymbol{X}_i) = \boldsymbol{W}_i^{*\mathrm{T}}\boldsymbol{\theta}_i(\boldsymbol{X}_i) + \phi_i$$

where $\boldsymbol{X}_i = [\boldsymbol{q}_{ei}^{\mathrm{T}}, \boldsymbol{v}_{ei}^{\mathrm{T}}, \boldsymbol{v}_{1i}^{\mathrm{T}}, \boldsymbol{v}_{2i}^{\mathrm{T}}]^{\mathrm{T}} \in \mathbf{R}^{13}$; $\boldsymbol{X}_{i,j}$ implies the jth element of the vector $\boldsymbol{X}_i$; $\boldsymbol{\theta}_i(\boldsymbol{X}_i) = [1, \boldsymbol{N}_1(\boldsymbol{X}_{i,1}), \ldots, \boldsymbol{N}_p(\boldsymbol{X}_{i,1}), \ldots, \boldsymbol{N}_1(\boldsymbol{X}_{i,13}), \ldots, \boldsymbol{N}_p(\boldsymbol{X}_{i,13})]^{\mathrm{T}} \in \mathbf{R}^{13p+1}$ is the CNN basis function with p being the order of Chebyshev polynomials; $\boldsymbol{W}_i^* \in \mathbf{R}^{3\times 14p+1}$ denotes the optimal approximation weight matrix of the output layer. The Chebyshev polynomials can be obtained by using the two-term recursive formula given by

$$\begin{cases} \boldsymbol{N}_{m+1}(\boldsymbol{X}_{i,j}) = 2\boldsymbol{X}_{i,j}\boldsymbol{N}_m(\boldsymbol{X}_{i,j}) - \boldsymbol{N}_{m-1}(\boldsymbol{X}_{i,j}) \\ \boldsymbol{N}_1(\boldsymbol{X}_{i,j}) = \boldsymbol{X}_{i,j} \\ \boldsymbol{N}_0(x) = 1 \end{cases} \tag{22}$$

Assumption 5. The optimal function approximation is bounded so that $\mathrm{tr}(\boldsymbol{W}^{*\mathrm{T}}\boldsymbol{W}^*) \leqslant \overline{W}^*$, where $\overline{W}^*$ is a positive constant.

It is clear that as the states of the closed-loop system are driven to the reference trajectory, $\boldsymbol{q}_{ei}$ and $\boldsymbol{v}_{ei}$ converge to zero, and the uncertain term $\boldsymbol{D}_i(\cdot)$ will converge to the reference nonlinear function $\boldsymbol{D}_r(\cdot) = \boldsymbol{Q}_{ei}\boldsymbol{J}_i^{-1}(\boldsymbol{v}_{1i}^{\times}\boldsymbol{J}_i\boldsymbol{v}_{1i} + \boldsymbol{J}_i\boldsymbol{v}_{2i} + \boldsymbol{d}_i)$. Assumptions 1–5 show that the CNN approximation error denoted as ϕ_i is bounded such that $|\phi_i| \leqslant \bar{\phi}$, where $\bar{\phi}$ is a positive constant.

To facilitate the backstepping command filter technique, an auxiliary system is introduced:

$$\boldsymbol{z}_{1i} = \boldsymbol{q}_{ei} - \boldsymbol{\xi}_{1i} \tag{23}$$

$$\boldsymbol{z}_{2i} = \boldsymbol{v}_{ei} - \boldsymbol{\xi}_{2i} - \boldsymbol{\vartheta}_i \tag{24}$$

where $\boldsymbol{\vartheta}_i$ is the virtual control input; $\boldsymbol{\xi}_{1i}$ and $\boldsymbol{\xi}_{2i}$ are applied to obtain the saturated control law.

We denote $\Delta\boldsymbol{u}_i = \boldsymbol{u}_{0i} - \boldsymbol{u}_i$ as the extra part of control signal, which should be compensated in the design procedure. For this purpose, $\boldsymbol{\xi}_{1i}$ and $\boldsymbol{\xi}_{2i}$ are defined in the form of command filter:

$$\dot{\boldsymbol{\xi}}_{1i} = \boldsymbol{\xi}_{2i} - \eta_1\boldsymbol{\xi}_{1i} \tag{25}$$

$$\dot{\boldsymbol{\xi}}_{2i} = -\eta_2\boldsymbol{\xi}_{2i} + \boldsymbol{g}_0(\boldsymbol{q}_{ei})\Delta\boldsymbol{u}_i \tag{26}$$

where η_1 and η_2 are positive constants to be selected. With the filter Eqs. (25) and (26), $\Delta\boldsymbol{u}_i$ is involved in system analysis so that the saturated control law can be verified explicitly.

The saturated attitude coordinated tracking control algorithm with the adaptive tuning law for estimating the optimal weight matrix is proposed:

$$\begin{aligned} \boldsymbol{u}_i = \boldsymbol{g}_0(\boldsymbol{q}_{ei})^{-1}[&-\widehat{\boldsymbol{W}}_i^{\mathrm{T}}\boldsymbol{\theta}_i - \eta_2\boldsymbol{\xi}_{2i} + \dot{\boldsymbol{\vartheta}}_i - \boldsymbol{z}_{1i} - h_1\boldsymbol{z}_{2i} - h_2(\boldsymbol{z}_{2i} \\ &- \boldsymbol{z}_{2i}(t-T)) - h_3\sum_{j=1}^{n}a_{ij}(\boldsymbol{\xi}_{1i}(t-T) - \boldsymbol{\xi}_{1j}(t-T))] \end{aligned} \tag{27}$$

$$\dot{\widehat{\boldsymbol{W}}}_i = \gamma\boldsymbol{z}_{2i}^{\mathrm{T}}\boldsymbol{\theta}_i - \mu\gamma\widehat{\boldsymbol{W}}_i \tag{28}$$

where h_1, h_2, h_3, γ and μ are positive parameters; $\widehat{\boldsymbol{W}}_i$ is used to estimate the matrix $\boldsymbol{W}_i^*$. Let $\tilde{\boldsymbol{W}}_i = \boldsymbol{W}_i^* - \widehat{\boldsymbol{W}}_i$ denote the weight matrix estimation error.

Theorem 2. *Considering spacecraft formation governed by Eqs. (1)–(3), if control law defined as Eqs. (27) and (28) is adopted and system parameters are selected to satisfy inequalities (29)–(31),*

$$h_1 + h_2 - h_3\lambda_{\max}(\boldsymbol{L}\boldsymbol{L}^{\mathrm{T}}) - \frac{1}{2}(1 - \dot{T}) + \frac{h_2}{2(1-\dot{T})} > 0 \tag{29}$$

$$\eta_1 - \frac{1}{2} - \frac{1}{2}h_3 - \frac{1}{2}\eta_1^2h_3T^2 - \frac{1}{2}\eta_1h_3T^2 > 0 \tag{30}$$

$$\eta_2 - 1 - \frac{1}{2}\eta_1h_3T^2 - \frac{1}{2}h_3T^2 > 0 \tag{31}$$

Then, the trajectory of the closed-loop system can be guaranteed to be uniformly ultimately bounded (UUB).

Proof. In order to derive the virtual control signal, the Lyapunov candidate function is selected:

$$V_{\mathrm{a}}=\frac{1}{2}\sum_{i=1}^{n}z_{1i}^{\mathrm{T}}z_{1i} \tag{32}$$

Its time derivative is

$$\begin{aligned}\dot{V}_{\mathrm{a}}&=\sum_{i=1}^{n}z_{1i}^{\mathrm{T}}\dot{z}_{1i}=\sum_{i=1}^{n}z_{1i}^{\mathrm{T}}(v_{ei}-\xi_{2i}+\eta_1\xi_{1i})\\&=\sum_{i=1}^{n}z_{1i}^{\mathrm{T}}(z_{2i}+\vartheta_i+\eta_1\xi_{1i})\end{aligned} \tag{33}$$

Let the virtual control be $\vartheta_i=-\eta_1 q_{ei}$, and thus it leads to

$$\dot{V}_{\mathrm{a}}=z_1^{\mathrm{T}}z_2-\eta_1 z_1^{\mathrm{T}}q_{\mathrm{e}}+\eta_1 z_1^{\mathrm{T}}\xi_1=z_1^{\mathrm{T}}z_2-\eta_1 z_1^{\mathrm{T}}z_1 \tag{34}$$

where $\xi_1=[\xi_{11},\xi_{12},\ldots,\xi_{1n}]^{\mathrm{T}}$, $z_1=[z_{11},z_{12},\ldots,z_{1n}]^{\mathrm{T}}$ and $z_2=[z_{21},z_{22},\ldots,z_{2n}]^{\mathrm{T}}$. Then, considering Eqs. (24) and (26), we can obtain the following equation:

$$\begin{aligned}\dot{z}_{2i}&=D_i(\cdot)+g_0(q_{ei})u_{0i}+\eta_2\xi_{2i}-g_0(q_{ei})\Delta u_i-\dot{\vartheta}_i\\&=D_i(\cdot)+g_0(q_{ei})u_i+\eta_2\xi_{2i}-\dot{\vartheta}_i\end{aligned} \tag{35}$$

In view of Eq. (35), taking the control signal u_i designed as Eq. (27) into system stability analysis directly is possible and reasonable. □

Then, to show the stability of z_{2i} and $\tilde{W}_i$, a Lyapunov function is constructed as

$$V_{\mathrm{b}}=\frac{1}{2}\sum_{i=1}^{n}z_{2i}^{\mathrm{T}}z_{2i}+\frac{1}{2\gamma}\mathrm{tr}(\tilde{W}^{\mathrm{T}}\tilde{W}) \tag{36}$$

where $W=[W_1,W_2,\ldots,W_n]^{\mathrm{T}}$, $\widehat{W}=[\widehat{W}_1,\widehat{W}_2,\ldots,\widehat{W}_n]^{\mathrm{T}}$, $\tilde{W}=[\tilde{W}_1,\tilde{W}_2,\ldots,\tilde{W}_n]^{\mathrm{T}}$. Substituting control law Eq. (27) and adaptive law Eq. (28) into Eq. (36) results in

$$\begin{aligned}\dot{V}_{\mathrm{b}}&=\sum_{i=1}^{n}z_{2i}^{\mathrm{T}}D_i(\cdot)-\sum_{i=1}^{n}z_{2i}^{\mathrm{T}}\widehat{W}_i^{\mathrm{T}}\theta_i-z_2^{\mathrm{T}}z_1-h_1z_2^{\mathrm{T}}z_2\\&\quad-h_2z_2^{\mathrm{T}}(z_2-z_2(t-T))\\&\quad-h_3z_{2i}^{\mathrm{T}}\sum_{j=1}^{n}a_{ij}(\xi_{1i}(t-T)-\xi_{1j}(t-T))-\frac{1}{\gamma}\mathrm{tr}(\tilde{W}^{\mathrm{T}}\dot{\widehat{W}})\\&=z_2^{\mathrm{T}}(\tilde{W}^{\mathrm{T}}\theta+\phi)-z_2^{\mathrm{T}}z_1-(h_1+h_2)z_2^{\mathrm{T}}z_2\\&\quad+h_2z_2^{\mathrm{T}}z_2(t-T)-h_3z_2^{\mathrm{T}}L\xi_1\\&\quad+h_3z_2^{\mathrm{T}}L\int_{t-T}^{t}\dot{\xi}_1\mathrm{d}\sigma-\frac{1}{\gamma}\mathrm{tr}[\tilde{W}^{\mathrm{T}}(\gamma z_2^{\mathrm{T}}\theta-\mu\gamma\widehat{W})]\\&\leqslant-z_2^{\mathrm{T}}z_1-(h_1+h_2-h_3\lambda_{\max}(LL^{\mathrm{T}}))z_2^{\mathrm{T}}z_2\\&\quad+h_2z_2^{\mathrm{T}}z_2(t-T)+\frac{1}{2}h_3\xi_1^{\mathrm{T}}\xi_1\\&\quad+\frac{1}{2}h_3\left(\int_{t-T}^{t}\dot{\xi}_1\mathrm{d}\sigma\right)^{\mathrm{T}}\left(\int_{t-T}^{t}\dot{\xi}_1\mathrm{d}\sigma\right)+\|z_2\|\bar{\phi}+\mu\mathrm{tr}(\tilde{W}^{\mathrm{T}}\widehat{W})\end{aligned} \tag{37}$$

Due to the fact that

$$\begin{aligned}\mathrm{tr}(\tilde{W}^{\mathrm{T}}\widehat{W})&=\mathrm{tr}(\tilde{W}^{\mathrm{T}}W^{*})-\mathrm{tr}(\tilde{W}^{\mathrm{T}}\tilde{W})\\&\leqslant\frac{1}{2}\mathrm{tr}(W^{*\mathrm{T}}W^{*})-\frac{1}{2}\mathrm{tr}(\tilde{W}^{\mathrm{T}}\tilde{W})\leqslant\frac{1}{2}\overline{W}^{*}\end{aligned} \tag{38}$$

$$\left(\int_{t-T}^{t}\dot{\xi}_1\mathrm{d}\sigma\right)^{\mathrm{T}}\left(\int_{t-T}^{t}\dot{\xi}_1\mathrm{d}\sigma\right)\leqslant T\int_{t-T}^{t}\dot{\xi}_1^{\mathrm{T}}\dot{\xi}_1\mathrm{d}\sigma \tag{39}$$

Hence, Eq. (37) further leads to

$$\begin{aligned}\dot{V}_{\mathrm{b}}&\leqslant-z_2^{\mathrm{T}}z_1-(h_1+h_2-h_3\lambda_{\max}(LL^{\mathrm{T}}))z_2^{\mathrm{T}}z_2+h_2z_2^{\mathrm{T}}z_2(t-T)\\&\quad+\frac{1}{2}h_3\xi_1^{\mathrm{T}}\xi_1+\frac{1}{2}h_3T\int_{t-T}^{t}\dot{\xi}_1^{\mathrm{T}}\dot{\xi}_1\mathrm{d}\sigma+\|z_2\|\bar{\phi}+\frac{1}{2}\mu\overline{W}^{*}\end{aligned} \tag{40}$$

In addition, ξ_{1i} and ξ_{2i} should be taken into account to guarantee stability of the closed-loop system. Thus, we choose a Lyapunov function V_{c} as

$$V_{\mathrm{c}}=\frac{1}{2}\xi_1^{\mathrm{T}}\xi_1+\frac{1}{2}\xi_2^{\mathrm{T}}\xi_2 \tag{41}$$

where $\xi_2=[\xi_{21},\xi_{22},\ldots,\xi_{2n}]^{\mathrm{T}}$ is defined. Taking the time derivative of V_c along the command filter (25) and (26), we have

$$\begin{aligned}\dot{V}_{\mathrm{c}}&=\xi_1^{\mathrm{T}}\xi_2-\eta_1\xi_1^{\mathrm{T}}\xi_1-\eta_2\xi_2^{\mathrm{T}}\xi_2+\xi_2^{\mathrm{T}}g_0(q_{\mathrm{e}})\Delta u\\&\leqslant-\left(\eta_1-\frac{1}{2}\right)\xi_1^{\mathrm{T}}\xi_1-(\eta_2-1)\xi_2^{\mathrm{T}}\xi_2\\&\quad+\frac{1}{2}\Delta u^{\mathrm{T}}g_0(q_{\mathrm{e}})^{\mathrm{T}}g_0(q_{\mathrm{e}})\Delta u\end{aligned} \tag{42}$$

where $g_0(q_{\mathrm{e}})=\mathrm{diag}(g_0(q_{\mathrm{e}1}),g_0(q_{\mathrm{e}2}),\ldots,g_0(q_{en}))$, $\Delta u=[\Delta u_1,\Delta u_2,\ldots,\Delta u_n]^{\mathrm{T}}$.

Moreover, considering the communication delays, we adopt the following Lyapunov-Krasovskii candidate:

$$V_{\mathrm{d}}=\frac{1}{2}h_2\int_{t-T}^{t}z_2^{\mathrm{T}}z_2\mathrm{d}\sigma+\frac{1}{2}h_3T\int_{-T}^{0}\int_{t+\zeta}^{t}\dot{\xi}_1^{\mathrm{T}}\dot{\xi}_1\mathrm{d}\sigma\mathrm{d}\zeta \tag{43}$$

The time derivative of V_{d} along Eqs. (24) and (25) is given by

$$\begin{aligned}\dot{V}_{\mathrm{d}}&=\frac{1}{2}(1-\dot{T})h_2z_2^{\mathrm{T}}z_2-\frac{1}{2}(1-\dot{T})h_2z_2^{\mathrm{T}}(t-T)z_2(t-T)\\&\quad-\frac{1}{2}h_3T\int_{t-T}^{t}\dot{\xi}_1^{\mathrm{T}}\dot{\xi}_1\mathrm{d}\sigma+\frac{1}{2}h_3T^2\dot{\xi}_1^{\mathrm{T}}\dot{\xi}_1\\&\leqslant\frac{1}{2}(1-\dot{T})h_2z_2^{\mathrm{T}}z_2-\frac{1}{2}(1-\dot{T})h_2z_2^{\mathrm{T}}(t-T)z_2(t-T)\\&\quad-\frac{1}{2}h_3T\int_{t-T}^{t}\dot{\xi}_1^{\mathrm{T}}\dot{\xi}_1\mathrm{d}\sigma+\frac{1}{2}(\eta_1^2+\eta_1)h_3T^2\xi_1^{\mathrm{T}}\xi_1\\&\quad+\frac{1}{2}(\eta_1+1)h_3T^2\xi_2^{\mathrm{T}}\xi_2\end{aligned} \tag{44}$$

To this end, the Lyapunov function for the closed-loop system is constructed as

$$V_2=V_{\mathrm{a}}+V_{\mathrm{b}}+V_{\mathrm{c}}+V_{\mathrm{d}} \tag{45}$$

Based on the analysis above, the time derivative of V_2 is easy to get:

$$\begin{aligned}\dot{V}_2&\leqslant-\varsigma_1z_1^{\mathrm{T}}z_1-\varsigma_2z_2^{\mathrm{T}}z_2+\|z_2\|\bar{\phi}-\varsigma_3\xi_1^{\mathrm{T}}\xi_1-\varsigma_4\xi_2^{\mathrm{T}}\xi_2+\frac{1}{2}\mu\overline{W}^{*}\\&\quad+\frac{1}{2}\Delta u^{\mathrm{T}}g_0(q_{\mathrm{e}})^{\mathrm{T}}g_0(q_{\mathrm{e}})\Delta u\\&\quad-h_2\left(\frac{1}{\sqrt{2(1-\dot{T})}}z_2-\sqrt{\frac{1-\dot{T}}{2}}z_2(t-T)\right)^{\mathrm{T}}\\&\quad\times\left(\frac{1}{\sqrt{2(1-\dot{T})}}z_2-\sqrt{\frac{1-\dot{T}}{2}}z_2(t-T)\right)\\&\leqslant-\varsigma_1z_1^{\mathrm{T}}z_1-\varsigma_2\left(z_2-\frac{\bar{\phi}}{\sqrt{2\varsigma_2}}\right)^{\mathrm{T}}\left(z_2-\frac{\bar{\phi}}{\sqrt{2\varsigma_2}}\right)\\&\quad-\varsigma_3\xi_1^{\mathrm{T}}\xi_1-\varsigma_4\xi_2^{\mathrm{T}}\xi_2+\Theta\end{aligned} \tag{46}$$

where ς_1, ς_2, ς_3, ς_4 and Θ are defined as the following:

$$\begin{cases} \varsigma_1 = \eta_1 \\ \varsigma_2 = h_1 + h_2 - h_3\lambda_{\max}(\boldsymbol{L}\boldsymbol{L}^{\mathrm{T}}) - \frac{1}{2}(1-\dot{T}) + \frac{h_2}{2(1-\bar{T})} \\ \varsigma_3 = \eta_1 - \frac{1}{2} - \frac{1}{2}h_3 - \frac{1}{2}\eta_1^2 h_3 T^2 - \frac{1}{2}\eta_1 h_3 T^2 \\ \varsigma_4 = \eta_2 - 1 - \frac{1}{2}\eta_1 h_3 T^2 - \frac{1}{2}h_3 T^2 \\ \Theta = \frac{1}{2}\bar{\phi}^2 + \frac{1}{2}\mu\overline{W}^* + \frac{1}{8}\bar{\delta}^2\|\Delta\boldsymbol{u}\|^2 \end{cases}$$

It implies that $\dot{V}_2 \leqslant 0$ if either of the following conditions holds $\|\boldsymbol{z}_1\| \leqslant \sqrt{\Theta/\varsigma_1}$, $\|\boldsymbol{z}_2\| \leqslant \sqrt{\Theta/\varsigma_2} + \frac{\bar{\phi}}{\sqrt{2\varsigma_2}}$, $\|\boldsymbol{\xi}_1\| \leqslant \sqrt{\Theta/\varsigma_3}$ and $\|\boldsymbol{\xi}_2\| \leqslant \sqrt{\Theta/\varsigma_4}$, which in turn presents that $\boldsymbol{z}_1$, $\boldsymbol{z}_2$, $\boldsymbol{\xi}_1$ and $\boldsymbol{\xi}_2$ are uniformly ultimately bounded (UUB). Hence, given the definition of the auxiliary system Eqs. (23) and (24) and the filter Eqs. (25) and (26), we come to the conclusion that the attitude errors $\boldsymbol{q}_{ei}$ and the angular velocity errors $\boldsymbol{\omega}_{ei}$ are UUB.

Remark 5. In fact, the magnitude of $\boldsymbol{u}$ decreases as the states of each spacecraft converge to the reference trajectory, which ensures that the final value of $\Delta\boldsymbol{u}$ is zero, i.e. $\lim_{t\to\infty}\Delta\boldsymbol{u} = \boldsymbol{0}$. Then, it can be deduced from Eq. (26) that $\boldsymbol{\xi}_2$ is asymptotically stable, and it also implies that $\boldsymbol{\xi}_1$ can achieve asymptotical stability from Eq. (25). Thus, system Eqs. (23) and (24) reduce to $\boldsymbol{z}_{1i} = \boldsymbol{q}_{ei}$ and $\boldsymbol{z}_{2i} = \boldsymbol{v}_{ei} - \vartheta_i$ after certain time, which is accordant with the conclusion of Theorem 2.

Remark 6. It should be mentioned that to construct the Lyapunov candidate function V_{d}, the communication delay T is used in Eq. (43). However, the appearance of unknown T is acceptable, which would not bring any trouble to control law design, because the exact value of T is related to the selection of control parameters rather than the structure of controller Eq. (27).

Remark 7. From the proof procedure, it is noticeable that the distributed control law defined as Eqs. (27) and (28) is free from the restriction of communication topology. Hence, the attitude coordinated tracking can be achieved only if Eqs. (29)–(31) are satisfied. Thus the condition on communication within the spacecraft formation is further relaxed.

4. Simulation and analysis

A formation of four spacecraft under a fixed directed communication topology is employed in the numerical work. Additionally, the performance of control algorithm in Ref. [35] has been examined as well, which is presented as below:

$$\boldsymbol{\tau}_i = -\lambda_i^p\boldsymbol{q}_{ei} - \lambda_i^d\boldsymbol{\omega}_{ei} - \frac{\lambda_i^i}{2}(q_{ei0}\boldsymbol{I} - \boldsymbol{q}_{ei}^{\times})\boldsymbol{\varepsilon}_{ei} + \boldsymbol{Y}_i\hat{\boldsymbol{\theta}}_i - \sum_{j=1}^{n}\left(\lambda_{ij}^{\mathrm{syn1}}\boldsymbol{\kappa}_{ei} - f_{ij}\lambda_{ij}^{\mathrm{syn2}}\boldsymbol{C}_{ij}(t-T_{ij})\boldsymbol{\kappa}_{ej}(t-T_{ij})\right) \quad (47)$$

where λ_i^p, λ_i^d, λ_i^i, $\lambda_{ij}^{\mathrm{syn1}}$, $\lambda_{ij}^{\mathrm{syn2}}$, f_{ij} are positive control parameters; $\boldsymbol{\Lambda}_i$ is a positive definite weighted matrix; T_{ij} represents the communication delays from the jth spacecraft to the ith spacecraft; $\boldsymbol{\kappa}_{ei} = \boldsymbol{\omega}_{ei} + c_i\boldsymbol{q}_{ei}$; $\dot{\boldsymbol{\varepsilon}}_{ei} = \frac{1}{2}q_{ei0}\boldsymbol{q}_{ei}$; $\dot{\hat{\boldsymbol{\theta}}}_i = -\boldsymbol{\Lambda}_i\boldsymbol{Y}_i^{\mathrm{T}}\boldsymbol{\kappa}_{ei}$; $\boldsymbol{Y}_i = (\boldsymbol{C}_{\mathrm{d}i}\boldsymbol{\omega}_{\mathrm{d}})^{\times}\boldsymbol{\Gamma}(\boldsymbol{C}_{\mathrm{d}i}\boldsymbol{\omega}_{\mathrm{d}}) + \boldsymbol{\Gamma}(\boldsymbol{C}_{\mathrm{d}i}\dot{\boldsymbol{\omega}}_{\mathrm{d}})$; $\boldsymbol{C}_{\mathrm{d}i} = \boldsymbol{C}_i\boldsymbol{C}_{\mathrm{d}}^{\mathrm{T}}$ denotes the rotation matrix from the desired reference frame to the body-fixed frame of the ith spacecraft; $\boldsymbol{C}_{ij}(t-T_{ij}) = \boldsymbol{C}_i\boldsymbol{C}_j^{\mathrm{T}}(t-T_{ij})$ denotes the delayed rotation matrix from the jth body reference frame to the ith body reference frame; $\boldsymbol{C}_i = (q_{i0}^2 - \boldsymbol{q}_i^{\mathrm{T}}\boldsymbol{q}_i)\boldsymbol{I}_{3\times3} + 2\boldsymbol{q}_i\boldsymbol{q}_i^{\mathrm{T}} - 2q_{i0}\boldsymbol{q}_i^{\times}$ and the definition of matrices $\boldsymbol{C}_i$ and $\boldsymbol{C}_j(t-T_{ij})$ can be deduced. Given a vector $\boldsymbol{x} = [(\boldsymbol{x})_1, (\boldsymbol{x})_2, (\boldsymbol{x})_3] \in \mathbf{R}^3$, the matrix $\boldsymbol{\Gamma}$ is defined as follows

$$\boldsymbol{\Gamma}(\boldsymbol{x}) = \begin{bmatrix} (\boldsymbol{x})_1 & (\boldsymbol{x})_2 & (\boldsymbol{x})_3 & 0 & 0 & 0 \\ 0 & (\boldsymbol{x})_1 & 0 & (\boldsymbol{x})_2 & (\boldsymbol{x})_3 & 0 \\ 0 & 0 & (\boldsymbol{x})_1 & 0 & (\boldsymbol{x})_2 & (\boldsymbol{x})_3 \end{bmatrix}, \quad \forall\boldsymbol{x} \in \mathbf{R}^3$$

Thus the improvement of the proposed control law can be verified. To ensure the fair comparison, the system states and communication topology for the proposed control laws and controller Eq. (47) are selected to be the same.

The initial attitudes, angular velocities and inertia matrices for each spacecraft are presented in Table 1. A virtual dynamic leader ξ^{r} provides reference trajectory for the multiple spacecraft formation, which rotates with the angular velocity of $\boldsymbol{\omega}_{\mathrm{d}} = [0.1\cos(0.01t), -0.1\sin(0.01t), -0.1\cos(0.01t)]^{\mathrm{T}}\mathrm{rad/s}$, and the initial attitude is chosen as $\bar{\boldsymbol{q}}_{\mathrm{d}}(0) = [0.8062, -0.1, 0.5, -0.3]^{\mathrm{T}}$. The communication topology is described in Fig. 1, where "SC1", "SC2", "SC3" and "SC4" represent the four spacecrafts in the formation. The communication time-delay between the neighboring spacecraft is supposed to be $T = 0.15\sin(0.02t)$s. Without loss of generality, the external disturbance is selected as

$$\boldsymbol{d}_i = [0.02\cos(0.02t), -0.03\cos(0.025t), 0.04\cos(0.03t)]^{\mathrm{T}}\mathrm{N}\cdot\mathrm{m} \quad (i = 1,2,3,4)$$

The response curves of closed-loop system by using controller Eq. (7) are carried out in Figs. 2–4. The control gains are selected as $\varepsilon = 0.5$, $\rho = 0.05$, $k_1 = 3$, $k_2 = 5$, $k_3 = 1$. Figs. 2 and 3 illustrate the absolute attitude errors and angular veloc-

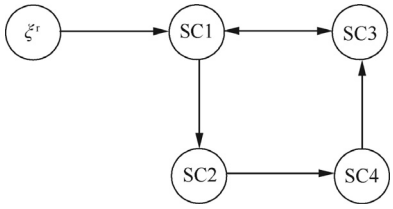

Fig. 1 Communication topology between spacecrafts.

Table 1 System parameters of spacecraft formation.

Spacecraft No.	Initial attitude	Initial angular velocity (rad/s)	Inertia moment (kg·m^2)
1	$\bar{\boldsymbol{q}}_1(0) = [0.5099 \quad -0.7 \quad -0.3 \quad -0.4]^{\mathrm{T}}$	$\boldsymbol{\omega}_1(0) = [0.13 \quad -0.15 \quad 0.1]^{\mathrm{T}}$	$\boldsymbol{J}_{01} = \mathrm{diag}(10.35, 9.67, 10.53)$
2	$\bar{\boldsymbol{q}}_2(0) = [0.5477 \quad 0.3 \quad -0.6 \quad -0.5]^{\mathrm{T}}$	$\boldsymbol{\omega}_2(0) = [-0.2 \quad 0.06 \quad 0.3]^{\mathrm{T}}$	$\boldsymbol{J}_{02} = \mathrm{diag}(10.95, 10.23, 11.16)$
3	$\bar{\boldsymbol{q}}_3(0) = [0.7874 \quad -0.3 \quad 0.5 \quad 0.2]^{\mathrm{T}}$	$\boldsymbol{\omega}_3(0) = [0.2 \quad -0.2 \quad -0.26]^{\mathrm{T}}$	$\boldsymbol{J}_{03} = \mathrm{diag}(11.79, 9.85, 10.58)$
4	$\bar{\boldsymbol{q}}_4(0) = [0.4796 \quad -0.4 \quad -0.6 \quad -0.5]^{\mathrm{T}}$	$\boldsymbol{\omega}_4(0) = [-0.04 \quad 0.12 \quad -0.06]^{\mathrm{T}}$	$\boldsymbol{J}_{04} = \mathrm{diag}(10.79, 11.85, 9.58)$

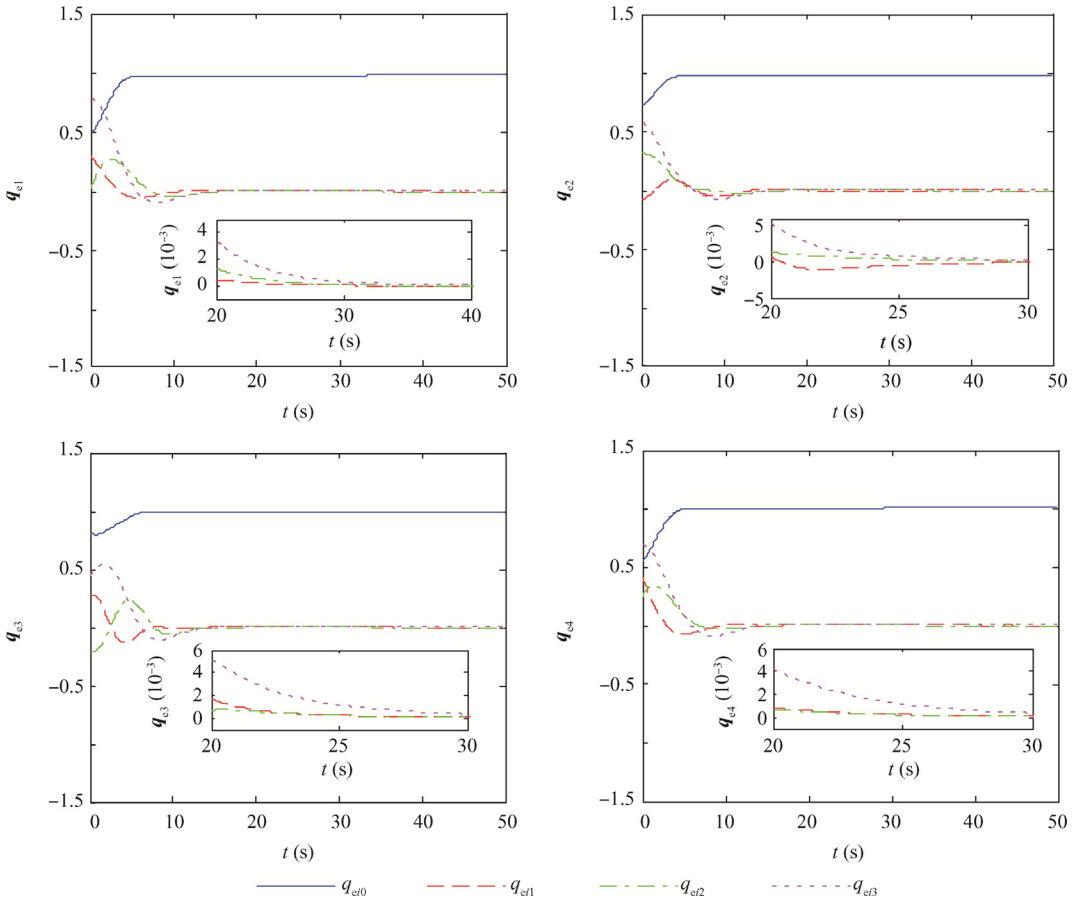

Fig. 2 Attitude errors of spacecraft formation under control law Eq. (7).

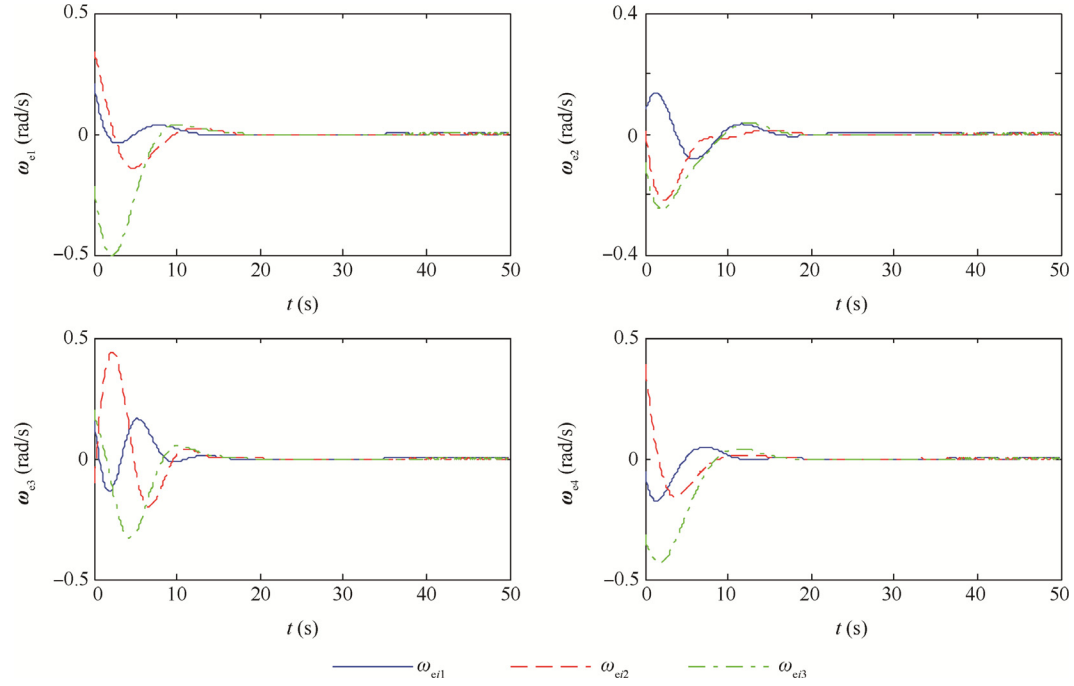

Fig. 3 Angular velocity errors of spacecraft formation under control law Eq. (7).

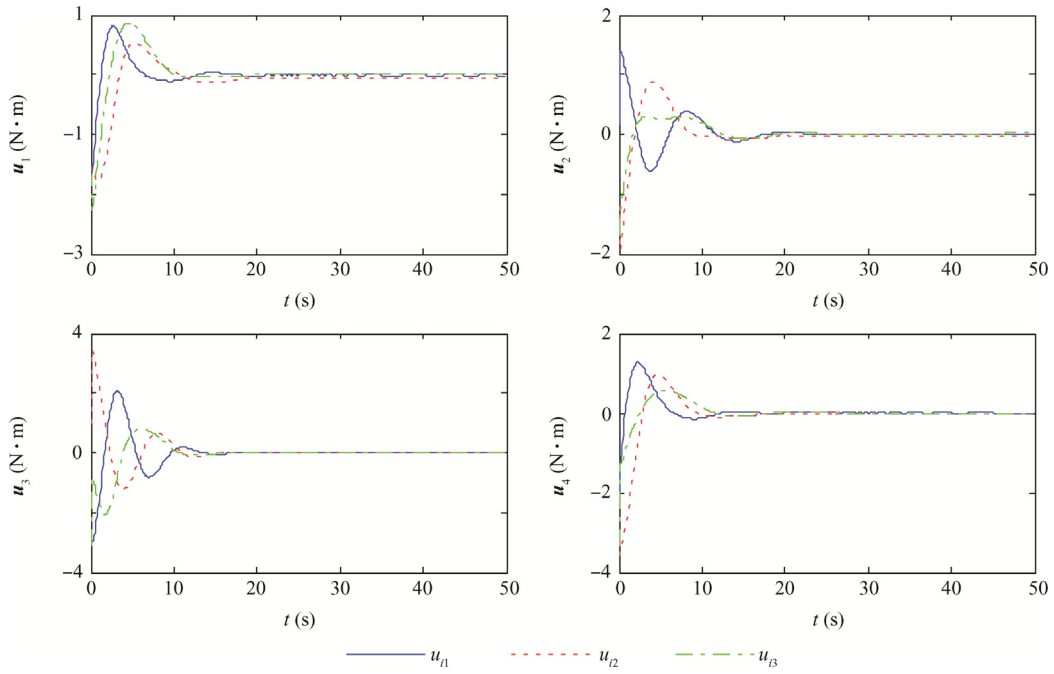

Fig. 4 Control torque of spacecraft formation under control law Eq. (7).

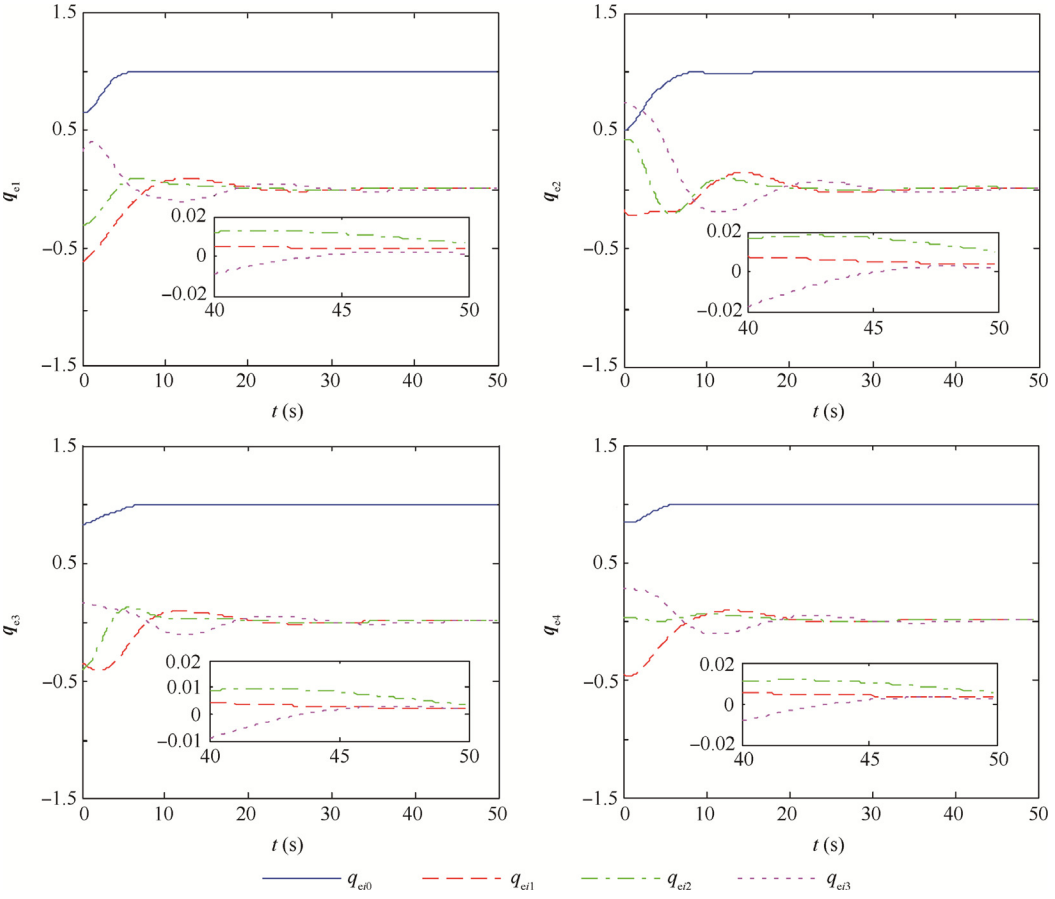

Fig. 5 Attitude errors of spacecraft formation under control law Eq. (47).

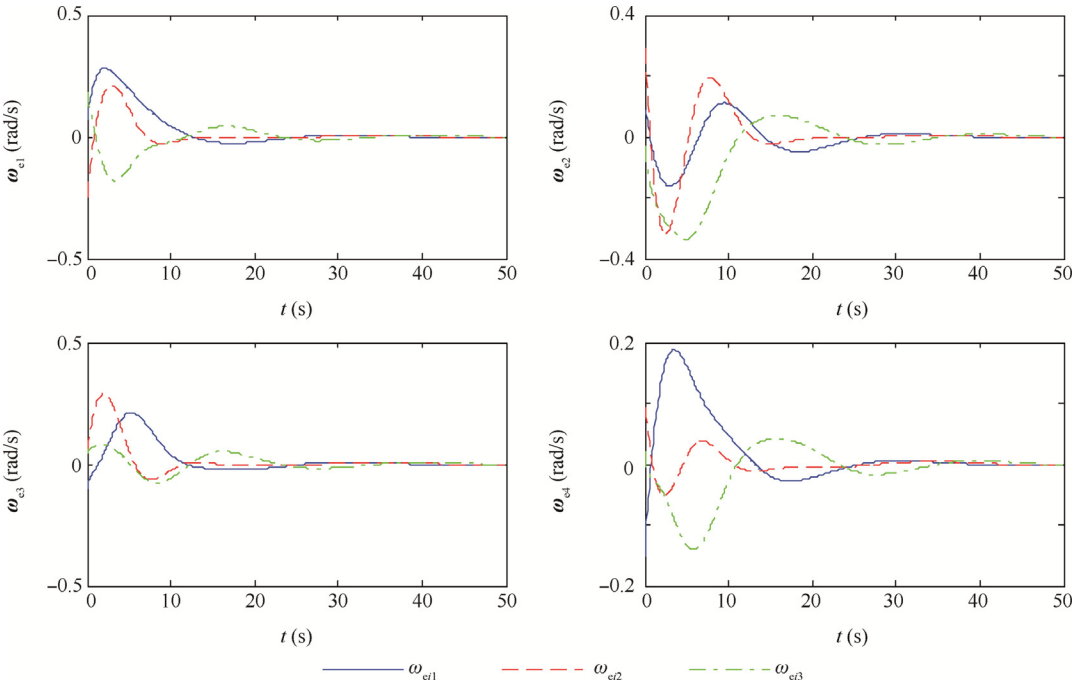

Fig. 6 Angular velocity errors of spacecraft formation under control law Eq. (47).

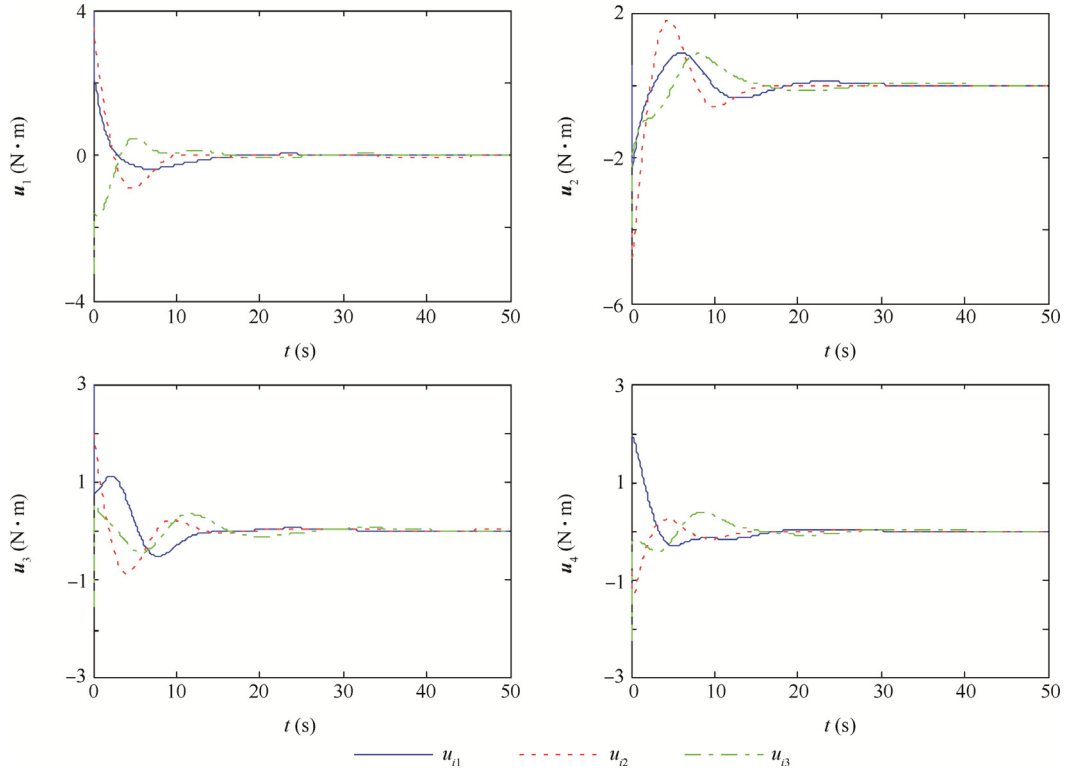

Fig. 7 Control torque of spacecraft formation under control law Eq. (47).

ity errors of each spacecraft. And it can be observed that the attitude tracking error converges to zero with the precision of $|q_{eiw}| < 6 \times 10^{-3}$ $(w = 1, 2, 3)$ in less than 20 s.

The performance of angular velocity tracking during the transient phase and the final accuracy are acceptable. The time history of the control torques under controller Eq. (7) is

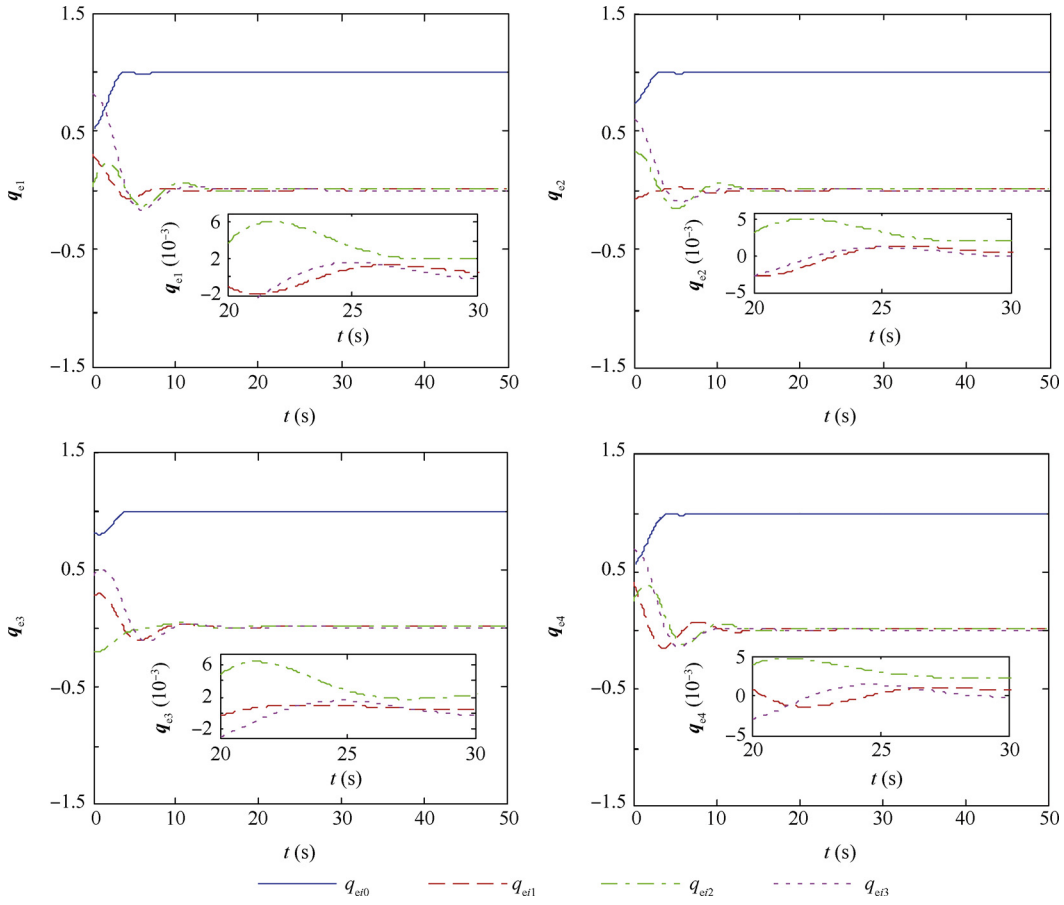

Fig. 8 Attitude errors of spacecraft formation under RSDDC.

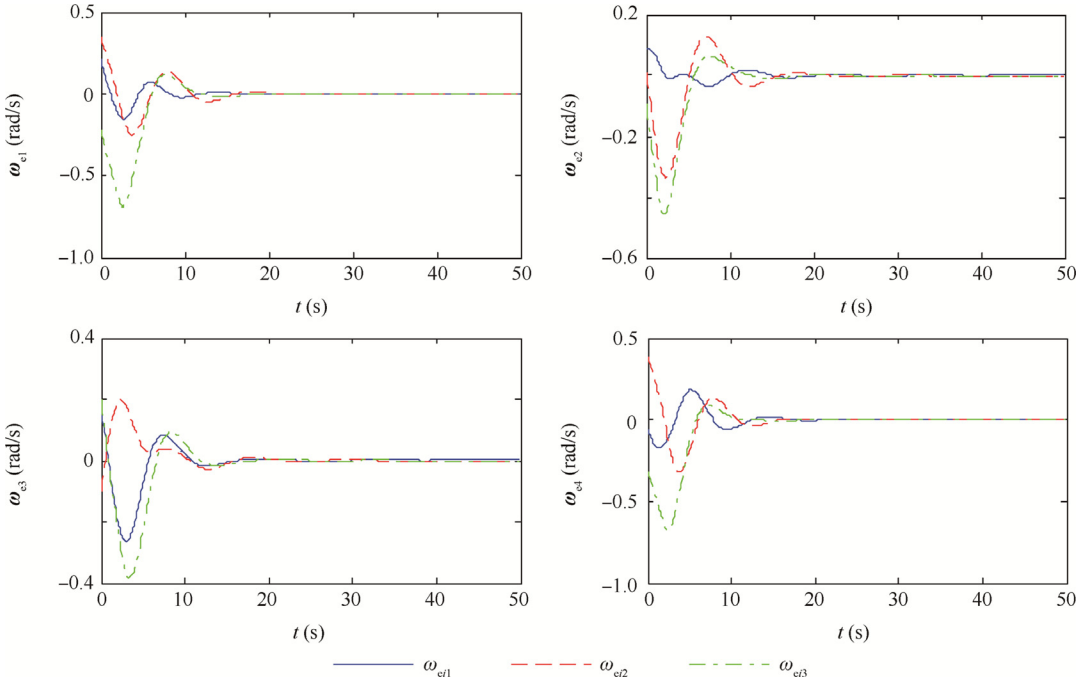

Fig. 9 Angular velocity errors of spacecraft formation under RSDDC.

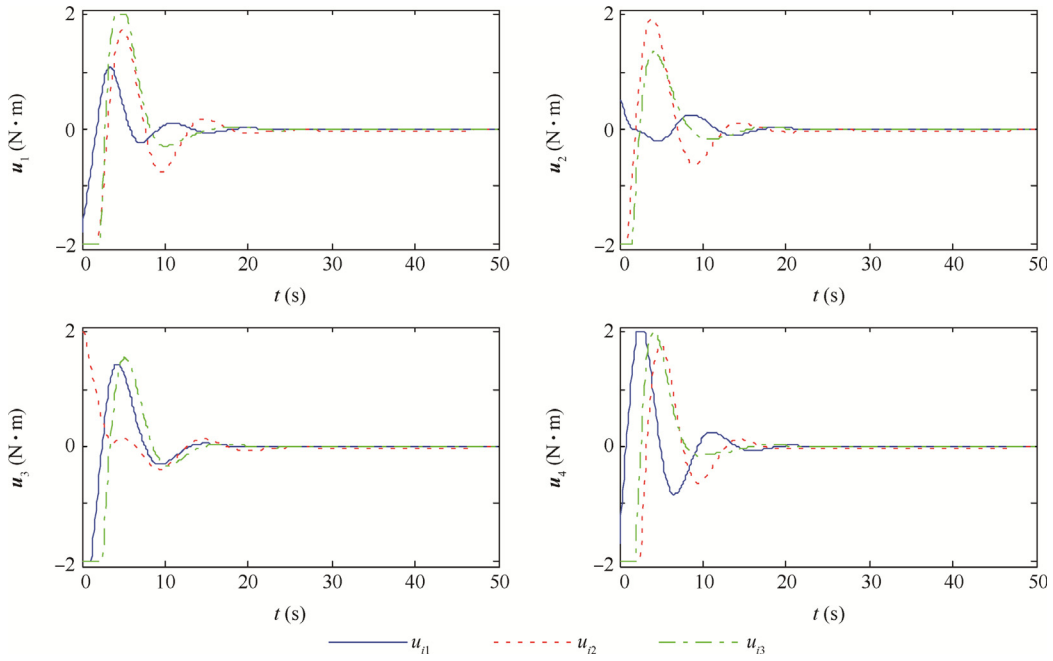

Fig. 10 Control torque of spacecraft formation under RSDDC.

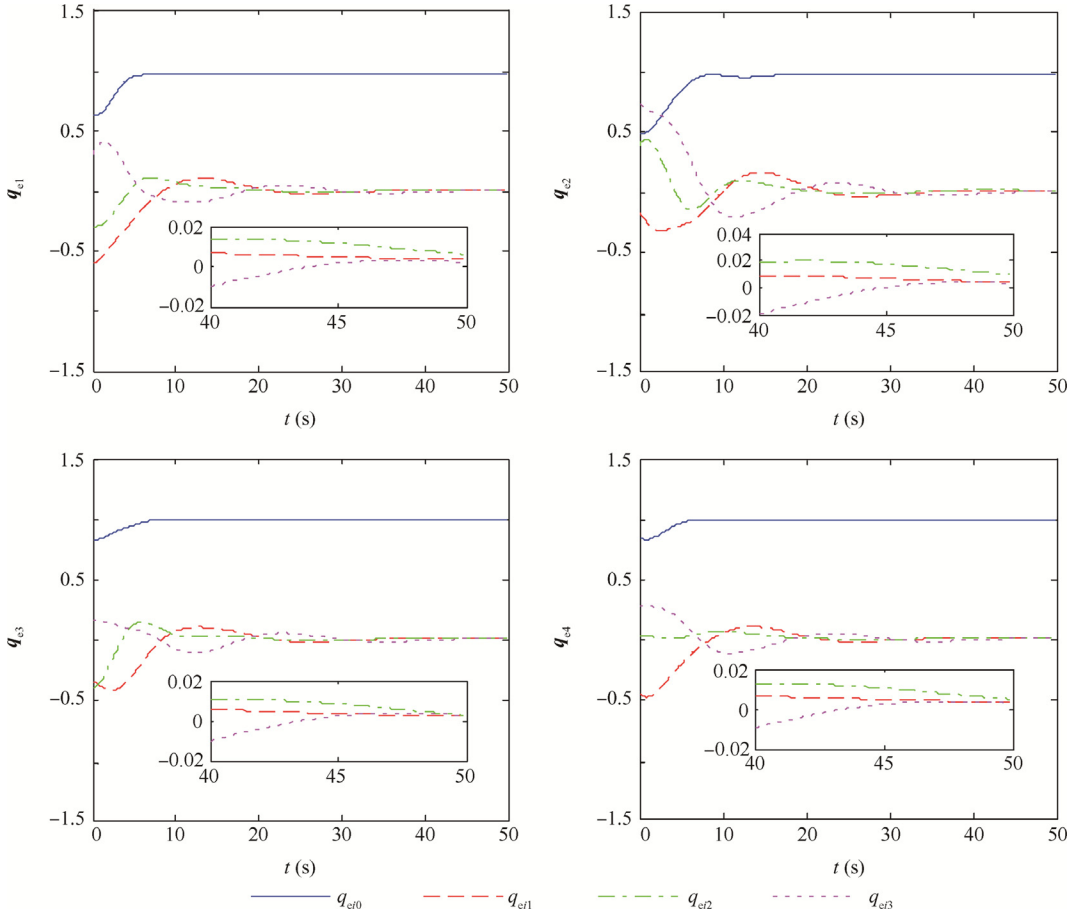

Fig. 11 Attitude errors of spacecraft formation under control law Eq. (47) with input saturation.

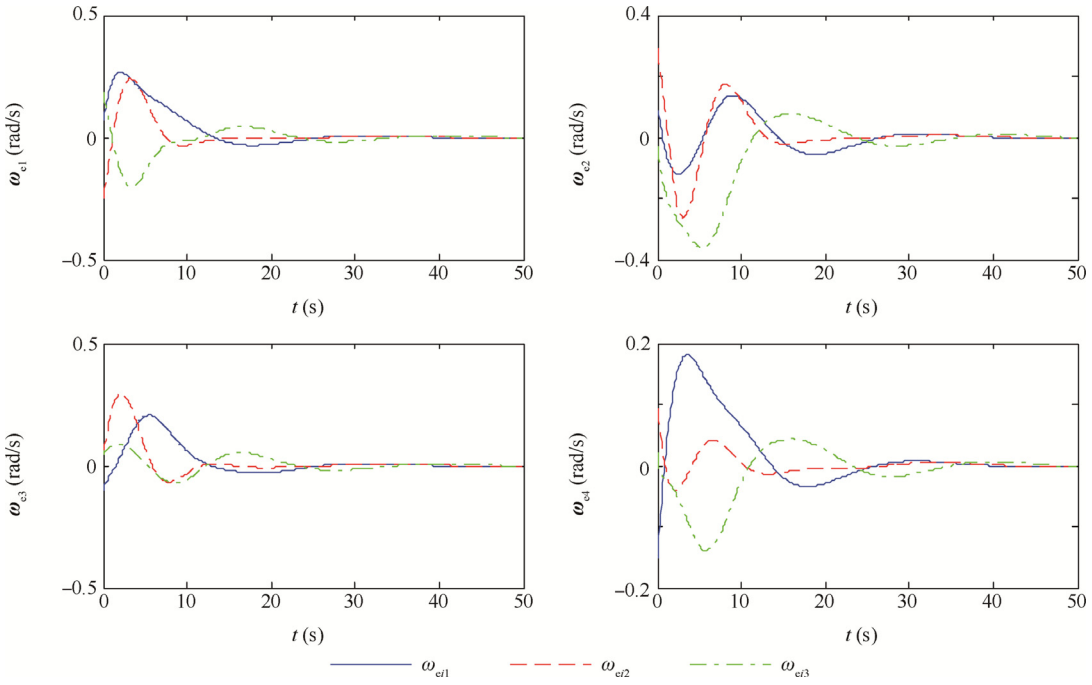

Fig. 12 Angular velocity errors of spacecraft formation under control law Eq. (47) with input saturation.

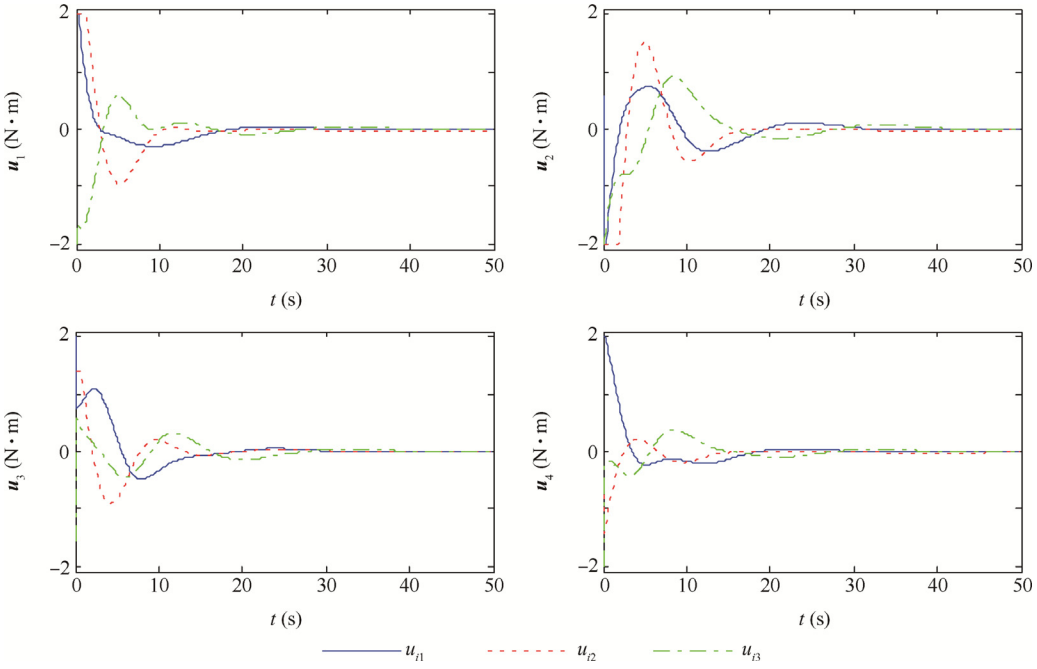

Fig. 13 Control torque of spacecraft formation under control law Eq. (47) with input saturation.

depicted in Fig. 4. As there is no restriction effect on the actuators, the magnitude generated by the control law reaches $|\boldsymbol{u}_{iw}|_{\max} = 4\ \mathrm{N}\cdot\mathrm{m}$ approximately.

Then, simulated results under controller Eq. (47) are shown in Figs. 5–7 with the control gains chosen as $c_i = 1$, $\lambda_i^p = 3.5$, $\lambda_i^d = 2$, $\lambda_i^i = 0.1$, $\lambda_{ij}^{\mathrm{syn1}} = 1$, $\lambda_{ij}^{\mathrm{syn2}} = 1$, $f_{ij} = 1$, $\boldsymbol{\Lambda}_i = 2\boldsymbol{I}$. From Fig. 5, it is observed that the attitude tracking errors drop to the attraction of $|q_{eiw}| < 2 \times 10^{-2}$ $(w = 1, 2, 3)$ within 40 s.

The corresponding angular velocity errors are given in Fig. 6, and the response curves of control torque are described in Fig. 7. Compared with the performance under control law Eq. (7), the final precision of attitude tracking has been reduced whereas the control torque remains the same level. Hence, the conclusion can be made that the proposed controller Eq. (7) guarantees better robustness and higher accuracy.

System performance under the robust saturated delay-dependent controller (denoted as RSDDC) is presented in Figs. 8–10. The control parameters are chosen as $\eta_1 = 5$, $\eta_2 = 1$, $h_1 = 1$, $h_2 = 0.5$, $h_3 = 0.1$, $\gamma = 0.1$, $\mu = 0.05$. The attitude tracking errors are presented in Fig. 8, from which it can be seen that the vector parts of $\boldsymbol{q}_{ei}$ drop to a small region around zero, i.e. $|q_{eiw}| < 7 \times 10^{-3}$ $(w = 1, 2, 3)$ at 20 s.

The angular velocity tracking errors are recorded in Fig. 9, correspondingly. Fig. 10 presents the actual control torque under the RSDDC with the maximum allowance of $\bar{u}_0 = 2\ \mathrm{N \cdot m}$. It shows that the control signals calculated by RSDDC have exceeded the given upper bound at the beginning. However, the actual control torque can be constrained within $\pm 2\ \mathrm{N \cdot m}$ during the whole simulating period. Then, control torques decrease into the allowable scope as the state errors illuminate, which reduce to a small region of zero finally. Although the control torque of the RSDDC has been cut down considerably compared with that in Fig. 4, system performance has not been degraded.

In order to compare system performance, the allowable bound of control torque generated by control law Eq. (47) should be set as same as that under RSDDC, i.e. $|u_{iw}|_{\max} = 2\ \mathrm{N \cdot m}$. The control parameters are chosen as the former case, and thus the work in the following Figs. 11–13 is carried out. The attitude tracking errors are shown in Fig. 11, which imply that the vector parts of quaternion converge to a close neighborhood around the equilibrium, i.e. $|q_{eiw}| < 2 \times 10^{-2}$ $(w = 1, 2, 3)$ at 40 s. The angular velocity errors are shown in Fig. 12, and the response curves of control torque with constraint are described in Fig. 13. It is observed that the control toque is restricted within $\pm 2\ \mathrm{N \cdot m}$ during the simulation period. However, the attitude tracking accuracy is apparently lower than that of RSDDC. Thus the superiority of the proposed robust saturated delay-dependent controller has been illustrated.

The effectiveness of the two attitude coordinated control laws for spacecraft formation with communication delays are verified by summarizing both cases above. Moreover, better robustness and faster response speed can be achieved by using the robust saturated control algorithm.

5. Conclusions

(1) The attitude coordinated tracking problem for the spacecraft formation is studied in this article, where inertia uncertainties, external disturbances, input saturation and communication time-delay are taken into accounted simultaneously.
(2) With the Lyapunov-Krasovskii approach, two attitude coordinated control laws are developed under the fixed directed topology, thus communication delays are explicitly addressed and overcome. Moreover, the delay-dependent control schemes reduce the conservatism of the concerned system.
(3) In addition, the time-delay between different formation members are supposed to be symmetrical, which limits the feasibility of the proposed algorithms. Hence, asymmetric communication delays and control strategies under switching topology will be further investigated in our future research work.

Acknowledgements

This study was co-supported by the National Natural Science Foundation of China (Nos. 61633003 and 61522301), Heilongjiang Province Science Foundation for Youths (Nos. QC2012C024 and QC2015064), and the Research Fund for Doctoral Program of Higher Education of China (No. 20132302110028).

References

1. Kristiansen R, Grotli EI, Nicklasson PJ, Gravdahl JT. A model of relative translation and rotation in leader-follower spacecraft formation. *Model Ident Control* 2007;**28**(1):3–13.
2. Jin ED, Jiang XL, Sun ZW. Robust decentralized attitude coordination control of spacecraft formation. *Syst Control Lett* 2008;**57**(7):567–77.
3. Cong BL, Liu XD, Chen Z. Distributed attitude synchronization of formation flying via consensus-based virtual structure. *Acta Astronaut* 2011;**68**(11–12):1973–86.
4. Abdessameud A, Tayebi A. Attitude synchronization of a group of spacecraft without velocity measurements. *IEEE Trans Autom Control* 2009;**54**(11):2642–8.
5. Yang HJ, You X, Xia YQ, Li HB. Adaptive control for attitude synchronisation of spacecraft formation via extended state observer. *IET Control Theory Appl* 2014;**8**(18):2171–85.
6. Zhang Z, Zhang ZX, Zhang H. Decentralized robust attitude tracking control for spacecraft networks under unknown inertia matrices. *Neurocomputing* 2015;**165**(1):202–10.
7. Du HB, Li SH. Attitude synchronization control for a group of flexible spacecraft. *Automatica* 2013;**50**(2):646–51.
8. Zou AM, Kumar KD, Hou ZG. Quaternion-based adaptive output feedback attitude control of spacecraft using Chebyshev neural networks. *IEEE Trans Neural Networks* 2010;**21**(9):1457–71.
9. Fazlyab AR, Saberi FF, Kabganian M. Adaptive attitude controller for a satellite based on neural network in the presence of unknown external disturbances and actuator faults. *Adv Space Res* 2016;**57**(1):367–77.
10. Zhao L, Jia YM. Neural network-based distributed adaptive attitude synchronization control of spacecraft formation under modified fast terminal sliding mode. *Neurocomputing* 2016;**171**(1):230–41.
11. de Ruiter AHJ. Adaptive spacecraft attitude tracking control with actuator saturation. *J Guid Control Dynam* 2010;**33**(5):1692–6.
12. Kanamori M. Anti-windup adaptive law for Euler-Lagrange systems with actuator saturation. *Proceedings of the 10th IFAC symposium on robot control*; 2012 Sep 5–7. Dubrovnik, Croatia. South Africa: IFAC; 2012. p. 875–80.
13. Su YX, Zheng CH. Globally asymptotic stabilization of spacecraft with simple saturated proportional-derivative control. *J Guid Control Dynam* 2011;**34**(6):1932–6.
14. Boskovic JD, Li SM, Mehra RK. Robust adaptive variable structure control of spacecraft under control input saturation. *J Guid Control Dynam* 2001;**24**(1):14–22.
15. Bustan D, Pariz N, Sani SKH. Robust fault-tolerant tracking control design for spacecraft under control input saturation. *ISA Trans* 2014;**53**(4):1073–80.
16. Loria A, Nijeijer H. Bounded output feedback tracking control of fully actuated Euler-Lagrange systems. *Syst Control Lett* 1998;**33**(3):151–61.
17. Zhang BQ, Song SM. Decentralized coordinated control for multiple spacecraft formation maneuvers. *Acta Astronaut* 2012;**74**(74):79–97.
18. Cheng YY, Du HB, He YG, Jia RT. Distributed finite-time attitude regulation for multiple rigid spacecraft via bounded control. *Inform Sci* 2016;**328**(20):144–57.

19. Hu QL, Zhang J. Bounded finite-time coordinated attitude control via output feedback for spacecraft formation. *J Aerosp Eng* 2014;**28**(5):0414129.
20. Zou AM, Kumar KD. Neural network-based distributed attitude coordination control for spacecraft formation flying with input saturation. *IEEE Trans Neural Networks Learn Syst* 2012;**23**(7):1155–62.
21. Li GM, Liu XD. Coordinated multiple spacecraft attitude control with communication time delays and uncertainties. *Chin J Aeronaut* 2012;**12**(52):698–708.
22. Zhou JK, Hu QL, Zhang YM, Ma GF. Decentralised adaptive output feedback synchronisation tracking control of spacecraft formation with time-varying delay. *IET Control Theory Appl* 2012;**25**(3):406–15.
23. Li SH, Du HB, Shi P. Distributed attitude control for multiple spacecraft with communication delays. *IEEE Trans Aerosp Electron Syst* 2014;**50**(3):1765–73.
24. Guo YH, Lu PL, Liu XD. Attitude coordination for spacecraft formation with multiple communication delays. *Chin J Aeronaut* 2015;**28**(2):527–34.
25. Min HB, Wang SC, Sun FC, Gao ZJ, Zhang JS. Decentralized adaptive attitude synchronization of spacecraft formation. *Syst Control Lett* 2012;**61**(1):238–46.
26. Yang HJ, You X, Xia YQ, Liu ZX. Nonlinear attitude tracking control for spacecraft formation with multiple delays. *Adv Space Res* 2014;**54**(4):759–69.
27. Du HB, Li SH. Attitude synchronization for flexible spacecraft with communication delays. *IEEE Trans Autom Control* 2016;**61**(11):3625–30.
28. Xu SY, Feng G, Zou Y, Huang J. Robust controller design of uncertain discrete time-delay systems with input saturation and disturbances. *IEEE Trans Autom Control* 2012;**57**(10):2604–9.
29. Abdessameud A, Tayebi A. Synchronization of networked Lagrangian systems with input constraints. *Proceedings of the 18th IFAC world congress*, 2011 Aug 28-Sep 2. Milano, Italy. South Africa: IFAC; 2011. p. 2382–7.
30. Wen JTY, Delgado KK. The attitude control problem. *IEEE Trans Autom Control* 1991;**36**(10):1148–62.
31. Ren W, Beard RW. Consensus seeking in multi-agent systems under dynamically changing interaction topologies. *IEEE Trans Autom Control* 2005;**50**(5):655–61.
32. Ramakrishnan K, Ray G. Delay-range-dependent stability criterion for interval time-delay systems with nonlinear perturbations. *Int J Autom Comput* 2011;**8**(1):141–6.
33. Barthe F. Optimal Young's inequality and its converse: a simple proof. *Geom Funct Anal* 1998;**8**(2):234–42.
34. Khalil HK. Nonlinear systems. 3rd ed. New Jersey: Prentice-Hall; 2002. p. 323–9.
35. Jin ED, Sun ZW. Robust attitude synchronisation controllers design for spacecraft formation. *IET Control Theory Appl* 2009;**3**(3):325–39.